Natural organic matter coating changes the role of iron oxides in carbon preservation in marine sediments

Yunru Chen[1,2]*, Heidi Taubner[1,3], Verena Heuer[1,3], Jenny Altun[1,3], Rianne van Kaam[1], Lars Robben[4,5,6], Wolfgang Bach[1,3], Lea C. Wunder[2], Graciana Willis-Poratti[7,8], Anna Helms[2], Sabine Kasten[1,3,9], Matthias Zabel[1], Kai-Uwe Hinrichs[1,3], Michael W. Friedrich[1,2]

1. MARUM-Center for Marine Environmental Sciences, University of Bremen, Bremen, Germany

2. Microbial Ecophysiology Group, Faculty of Biology/Chemistry, University of Bremen, Bremen, Germany

3. Faculty of Geosciences, University of Bremen, Bremen, Germany

4. Solid State Chemical Crystallography, Faculty of Biology/Chemistry, Bremen, Germany

5. Data Science Center, University of Bremen, Germany

6. MAPEX – Center for Materials and Processes, University of Bremen, Germany

7. Instituto Antártico Argentino, Buenos Aires, Argentina

8. Consejo Nacional de Investigaciones Científicas y Técnicas, Buenos Aires, Argentina

9. Alfred Wegener Institute Helmholtz Centre for Polar and Marine Research, Bremerhaven, Germany

*Corresponding author: yunruchen@marum.de

Abstract

Preservation of organic carbon (OC) in marine and terrestrial depositional settings is enhanced by the association between OC and reactive iron oxides. However, microbially mediated iron reduction in anoxic marine sediments may lead to the reductive dissolution of iron oxides and consequently to the remobilization of iron-associated organic matter. The underlying mechanism remains poorly studied. Here, we studied the interaction between ferrihydrite (Fh) and ^{13}C-acetate using incubations with marine surface sediments. We found that when iron reduction was inhibited, adding pure Fh protected 51% more acetate from degradation compared to the incubation without Fh addition. In contrast, adding natural organic matter (NOM)-coated Fh protected 102% more acetate, likely due to a larger surface area from smaller aggregate sizes. When iron reduction was occurring, we observed significant differences. While only a limited amount of Fh-associated ^{13}C-acetate was remobilized from uncoated Fh, 76% of the Fh-associated ^{13}C-acetate was remobilized from NOM-coated Fh and remineralized by microorganisms. These results suggest that natural organic matter coating strongly alters the aggregate size of iron oxides and increases their surface area, enhancing their capability to adsorb organic molecules. However, much of these adsorbed molecules is subsequently remobilized through microbially mediated iron reduction. Therefore, both aggregate structure and microbial processes dynamically controlled the fate of iron-associated organic matter, which need to be considered when assessing the role of iron oxides in long-term carbon preservation.

Introduction

On geological timescales, the burial of sedimentary organic carbon (OC) is a major regulator of atmospheric O_2 and CO_2 concentrations[1] and represents the largest long-term carbon sink on Earth, thereby exerting a profound influence on Earth's environmental conditions. In marine sediments, approximately 20 % of the total organic carbon (TOC) is tightly associated with reactive iron oxides, highlighting the critical role of these minerals in the preservation of carbon in marine sediments[2].

Lab incubations have shown that under aerobic conditions the bio-availability of organic molecules can be entirely limited when associated with iron oxides[3-5]. However, iron oxides are actively involved in diverse biogeochemical cycles in anoxic marine sediments[6, 7]. They can be reduced through microbially mediated processes, either biotically when they act as electron acceptors during anaerobic microbial respiration by iron-reducing microorganisms[8-14], or abiotically via reaction with hydrogen sulfide produced by sulfate-reducing microorganisms[6, 15-17]. Both biotic and abiotic iron reduction drive the reductive dissolution of iron oxides, which may weaken or even break the association between iron and OC, thereby remobilizing iron-associated OC. Such remobilization has been reported in marine sediments, especially in layers where active sulfate reduction drives sulfide production[18-21], yet the effect of different iron reduction processes on the remobilization of iron-associated OC remains poorly quantified.

Ferrihydrite (Fh) is a widely distributed poorly crystalline iron (oxyhydr)oxide in soils and sediments[22]. Its high specific surface area results in strong sorption capacity and high bioreactivity, making Fh a key player in the biogeochemical cycling of OC[23]. Consequently, Fh has been widely used in *in-vitro* incubation experiments to study interactions between iron oxides and OC, as well as how these interactions could be influenced by iron reduction[24-27]. However, in all these incubations, Fh was freshly synthesized in the laboratory and used in the incubations with a pristine surface, i.e., without any associated OC. This is rarely the case in the natural environments, where Fh, and other iron oxides, have high affinity to organic molecules and are found coated with natural organic matter (NOM) on its surface[28, 29]. The organic coating on iron oxides could significantly change their aggregation behavior, leading to smaller aggregate sizes[30-32] and higher specific surface area. This is likely to have a significant impact on the further interactions between iron oxides, organic molecules, and microorganisms; however, this remains largely unexplored.

Here, we studied the interactions between Fh, acetate, and microbial communities living in marine sediments, as well as how NOM coating on Fh could influence these

interactions. Acetate, a key intermediate in the anaerobic breakdown of NOM in marine sediments, was selected as a representative organic molecule due to its central role in the metabolism of anaerobic microorganisms, particularly iron- and sulfate-reducing microorganisms[33-35]. The degradation of ^{13}C-acetate was monitored during 14-day anoxic incubations of surface sediments from Cumberland Bay (South Georgia, sub-Antarctic) under the protection by Fh with and without microbial remobilization. Two incubation series with exactly the same treatments were performed in parallel using uncoated and NOM-coated Fh, respectively. We quantified the fate of ^{13}C-acetate by combining concentration and carbon isotopic composition measurements of dissolved inorganic carbon (DIC) and acetate with geochemical indicators of microbial activities, including Fe^{2+} and sulfide concentrations. Our hypotheses are: (1) NOM-coated Fh, which may potentially have smaller aggregate size, can adsorb more acetate and protect it from microbial degradation; (2) under anoxic conditions, microbially mediated iron reduction is capable of remobilizing Fh-associated acetate.

Results and discussion

Substantial adsorption of natural organic matter on ferrihydrite resulted in smaller aggregate size

To test adsorption characteristics of NOM and acetate on ferrihydrite (Fh), poorly crystalline Fh (2-line) was freshly synthesized and used in this study. Its structure was evaluated using X-ray diffraction. The diffraction data shows two broad reflections, consistent with previous studies (Supplementary Figure 1) [36]. Additionally, the reduced pair distribution function G(r) was calculated from the scattering data and refinements show a very good agreement with the structure models of Michel et al. for the quantumcrystalline 2-line Fh[37] (Supplementary Figure 2).

Natural organic matter (NOM) was extracted by shaking marine surface sediments with Milli-Q water (w:v = 1:6) for 24 h, followed by filtration through a 0.7 μm and a

0.22 µm filter to remove sediment particles and microorganisms. The sediments were collected from the so-called Confluence Zone, located in outer Cumberland Bay, South Georgia (MUC core PS133-2-42-9-4, 4-12 cmbsf, 54°12.521' S, 36°26.514' W) during the RV *Polarstern* expedition PS133-2 “Island Impact”() in November and December 2022[38], which were used for the incubation experiments as well. The NOM solution, with an initial dissolved organic carbon (DOC) concentration of 4.0 ± 0.4 mM, was mixed with 1 mmol Fh. After 24 hours, the DOC concentration reached equilibrium at 1.3 ± 0.1 mM (Supplementary Figure 3), and final NOM loading on Fh was 0.21 mol OC mol^{-1} Fh. Wagai and Mayer (2007) showed that the maximal adsorption capacity of NOM on goethite surface via single-layer adsorption has been estimated to result in a molar ratio of OC to iron of 1.0[39]. Considering that the lab-synthesized Fh generally has a higher specific surface area than goethite[40], which implies higher adsorption efficiency, the maximum molar ratio of adsorbed OC to Fh is expected to be at least 1.0. In our adsorption experiment, final NOM loading on Fh corresponded to an OC:iron molar ratio of only 0.2. This suggested that a substantial fraction of NOM was adsorbed to Fh within 24 hours, while some Fh surface area potentially remained available for further adsorption. The Fh after the adsorption experiment was collected and used as NOM-coated Fh in the subsequent incubations. A similar adsorption experiment was performed to determine the adsorption of acetate on fresh Fh. The acetate solution, with an initial concentration of 1.71 ± 0.02 mM, was mixed with 0.5 mmol Fh for 24 h. The adsorption of acetate was determined to be 0.03 mol acetate mol^{-1} Fh (Supplementary Figure 4).

To evaluate the chemical composition of NOM adsorbed on Fh, the absorbance and fluorescence characteristics of the NOM solution were determined before adsorption and of the supernatant after adsorption . The humification index (HIX), which is typically higher for terrestrial, humic-like NOM, decreased from 0.8 to 0.7 in the supernatant after adsorption, indicating a preferential adsorption of terrestrial humic-like NOM on Fh (Supplementary Figure 5 and Supplementary Data 1). This pattern is consistent with previous studies, indicating that highly unsaturated, aromatic

compounds enriched in carboxyl groups, which are characteristic of terrestrial humic-like NOM, exhibit a high affinity for Fh[41-43].

To assess whether Fh aggregation is affected by NOM coating and/or incubation with acetate, the structural characteristics of uncoated and NOM-coated Fh were analyzed. Samples were examined both before and after incubation with an acetate solution at a concentration of 120 μM. This preliminary assessment served to evaluate potential aggregation changes prior to and during the subsequent incubation experiments conducted under the same acetate concentration. The average crystallite size and its distribution were checked with total scattering experiments, and were very similar among uncoated Fh, NOM-coated Fh, and acetate-coated Fh (Supplementary Figure 6). This is expected, as the crystallite size of Fh is determined during synthesis and should not be affected by subsequent coating. The particle size distributions of uncoated and NOM-coated Fh were broadly similar (Supplementary Figure 7). NOM-coated Fh showed a greater proportion of particles in the range of 8 to 30 μm and fewer particles smaller than 8 μm and larger than 30 μm compared with uncoated Fh. Meanwhile, scanning electron microscope (SEM) micrographs clearly showed that NOM-coated Fh formed in general smaller aggregates than uncoated Fh (Figure 1). The aggregates of uncoated Fh were similar in size with and without incubation with acetate (Figure 1a and b), whereas NOM-coated Fh incubated with acetate had much smaller aggregates than uncoated Fh under same conditions (Figure 1b and c). These observations indicate that incubation with acetate solution does not affect aggregate size, while NOM coating substantially inhibits aggregation.

The carbon distribution on NOM-coated Fh incubated with acetate was further visualized by elemental mapping. The final loading of NOM and acetate on Fh after the adsorption experiments indicated that NOM contributes 4 times more carbon than acetate, the observed carbon signal largely reflects the NOM coating. This carbon is co-localized with iron across the particle surfaces, indicating that NOM is associated with the Fh aggregates (Figure 1d). The carbon map further highlights a

heterogeneous distribution, with localized enrichments suggesting patchy NOM coating on Fh surfaces (Figure 1e).

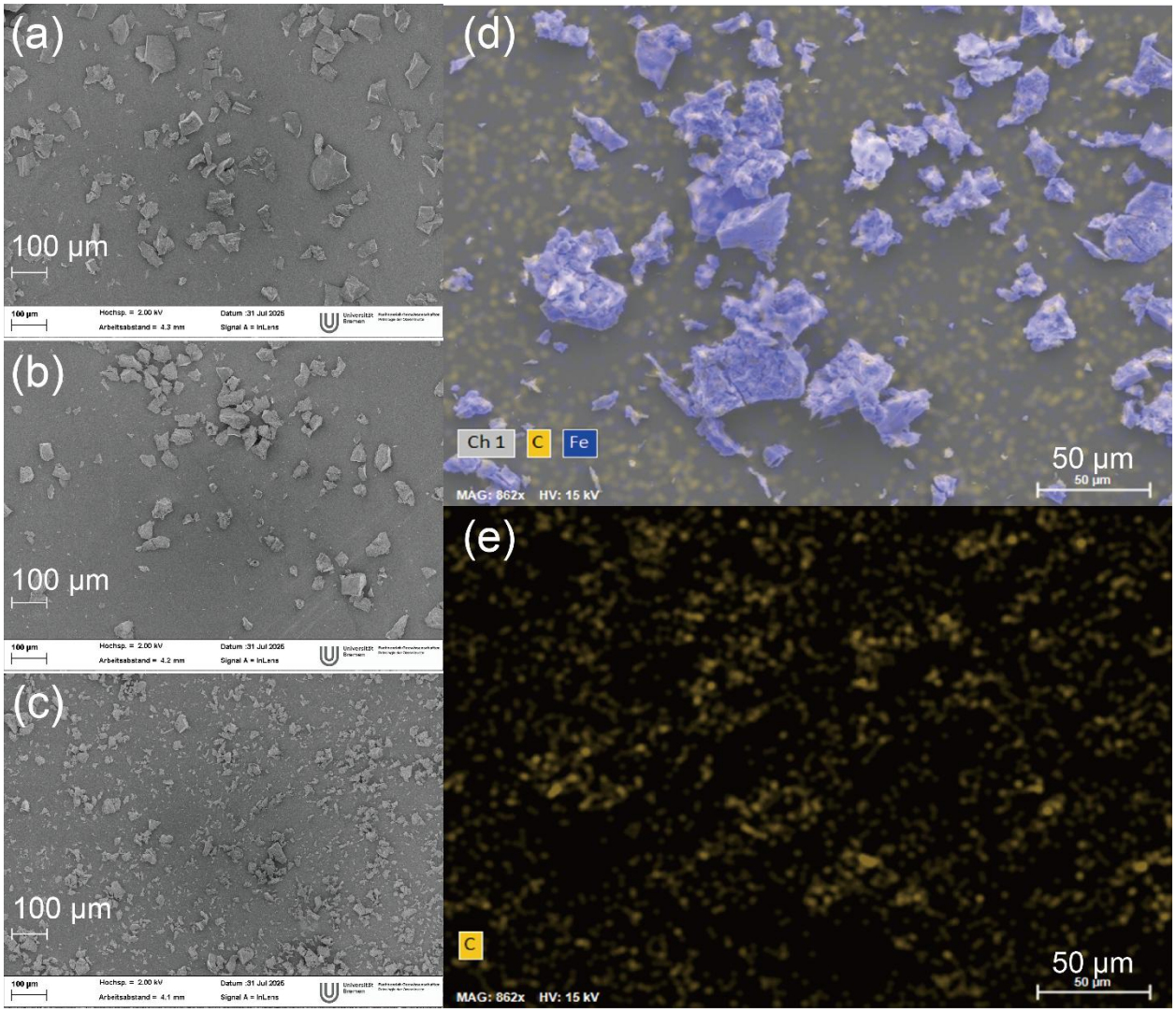

Figure 1. Morphology and carbon distribution on Fh after adsorption experiments with natural organic matter (NOM) and acetate. SEM micrographs show the aggregates of uncoated Fh (a), uncoated Fh incubated in acetate solution (b), and NOM-coated Fh incubated in acetate solution (c). Elemental maps show Fe and C distributions (d) and C distribution alone (e) on the surface of NOM-coated Fh incubated with acetate solution, where “Ch 1” represents the SEM micrographs of particle aggregates.

Microbially mediated iron reduction in uncoated and NOM-coated Fh incubations

Acetate is a suitable proxy for testing the role of iron oxides in protecting organic matter against degradation. If not protected, it can be readily used by microorganisms, including both iron-reducing and sulfate-reducing microorganisms[33-35]. In natural environments, iron oxides can readily become coated with NOM as iron oxides precipitate with the presence of NOM. Therefore, we used both uncoated and NOM-coated Fh (all referred to as "Fh" in the experimental set-up) to investigate the role of Fh in protecting acetate from degradation with and without microbial remobilization. ^{13}C-acetate was incubated anoxically with sediments from Cumberland Bay under three levels of protection by Fh: (1) no Fh protection, where no Fh was added to protect ^{13}C-acetate from microbial degradation; (2) full Fh protection, where Fh was added to protect ^{13}C-acetate and both biotic and abiotic iron reduction were inhibited to prevent microbial remobilization of adsorbed ^{13}C-acetate from Fh; and (3) partial Fh protection, where Fh was added to protect ^{13}C-acetate and biotic and/or abiotic iron reduction was allowed to counteract the effect of Fh protection on ^{13}C-acetate. (Figure 2, see Table 1 in methods for details).

In marine sediments, the concentration of acetate in pore water reflects a balance between rapid microbial production and consumption[44, 45]. Consequently, its concentrations in marine sediment pore water are typically low, ranging from a few hundred nanomolar to about a few hundred micromolar in most coastal and deep-sea settings[46-48]. In our incubation experiments, the acetate concentration was set at 120 µM, near the upper range of values found in natural sediment pore water. 1 mmol Fh, corresponding to 1.4 wt.-% of the dry sediment in the incubation system, was added. This is in the same range as the content of easily reducible iron oxides quantified in the Cumberland Bay sediments (0.2 wt.-% - 0.4 wt.-%) [49].

The microbial communities in the sediments used here are capable of conducting both biotic iron reduction by iron-reducing microorganisms and abiotic iron reduction by sulfide produced by sulfate-reducing microorganisms[50]. To disentangle the role of

biotic and abiotic iron reduction in remobilizing Fh-associated ^{13}C-acetate, different treatments were set up. To stop biotic iron reduction, Fh was added in incubations within a dialysis bag (molecular weight cutoff 12-14 kDa) to prevent the direct contract with microorganisms often required for biotic iron reduciton[51-53], while still allowing diffusion of low-molecular-weight compounds such as biogenic sulfide that can drive abiotic iron reduction. To suppress abiotic iron reduction through hydrogen sulfide, molybdate was added to inhibit sulfate reduction[50] (Figure 2).

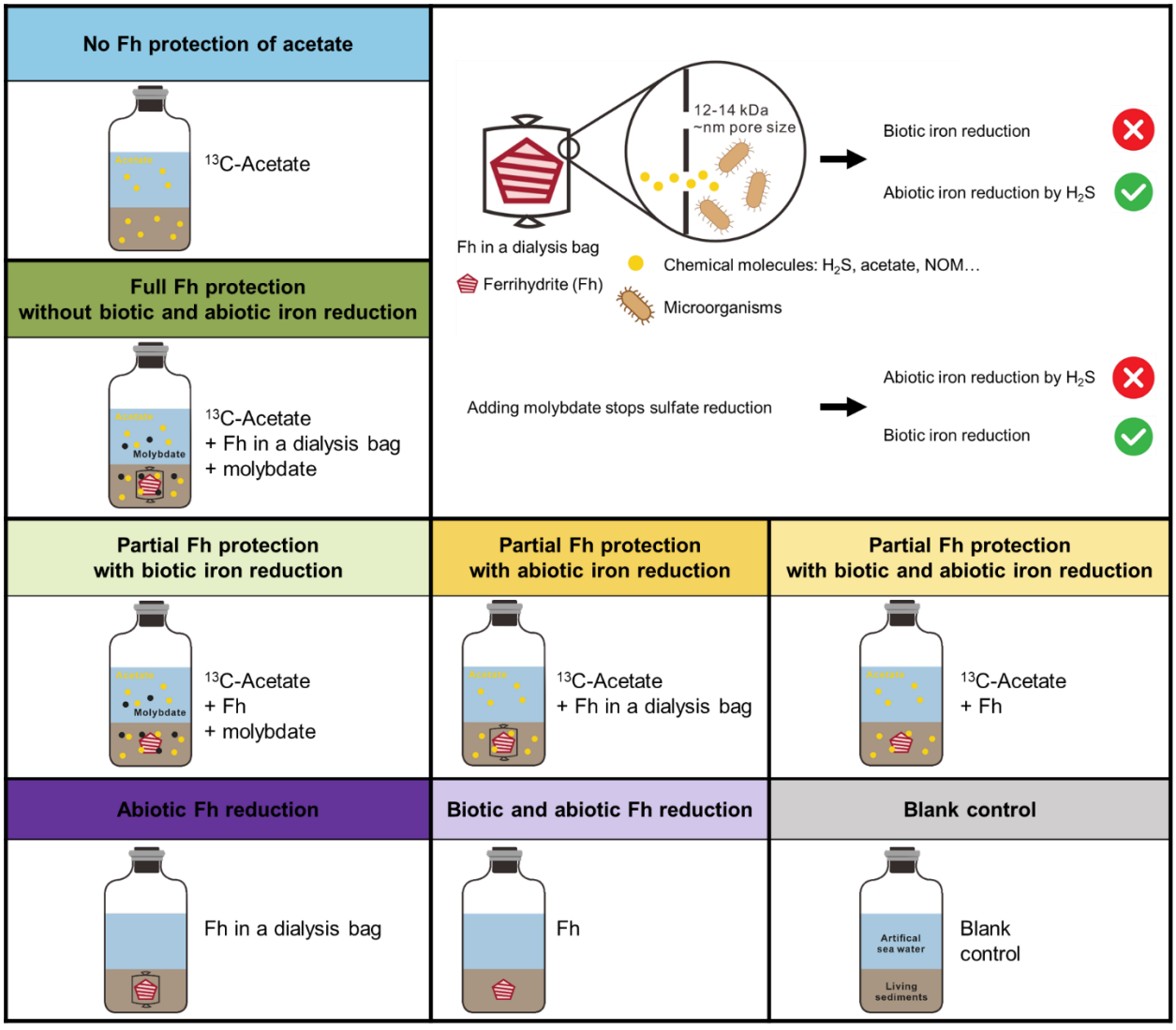

Figure 2. Conceptual schematic of the incubation set-up. Sediments were incubated with ^{13}C-acetate under three levels of Fh protection: no Fh protection, full

Fh protection inhibiting both biotic and abiotic iron reduction, and partial Fh protection allowing biotic and/or abiotic iron reduction. Fh protection refers to Fh protecting acetate from microbial degradation. The incubations were performed in parallel using uncoated Fh and NOM-coated Fh, respectively; both are referred to as “Fh” when describing the experimental set-up.

The Fe^{2+} and sulfide concentrations in the supernatant were measured to reflect iron and sulfate reduction throughout the incubation. In most treatments, Fe^{2+} concentrations fluctuated between 30 and 90 μM. In contrast, the sulfide concentrations stayed consistently low in all treatments, ranging from 0 to 5.3 μM. These results indicate co-occurring iron and sulfate reduction in all the treatments, except those with molybdate. The produced sulfide rapidly precipitates with Fe^{2+} and/or reacts with Fh, preventing the consistent accumulation of either species.

Stimulated iron reduction was observed in the treatments with NOM-coated Fh compared to the ones with uncoated Fh. This was likely due to the quick reduction of added Fh driven by the NOM coating (Figure 3). Besides, it was evident that physically isolating Fh in a dialysis bag effectively inhibited a substantial part of biotic iron reduction. This was especially reflected in the paired treatments with similar setups, where iron reduction was stimulated only when Fh was added directly into the incubations, but not when Fh was first put into a dialysis bag (Figure 3), corroborating that biotic iron reduction requires direct contact with mineral surface in our incubations.

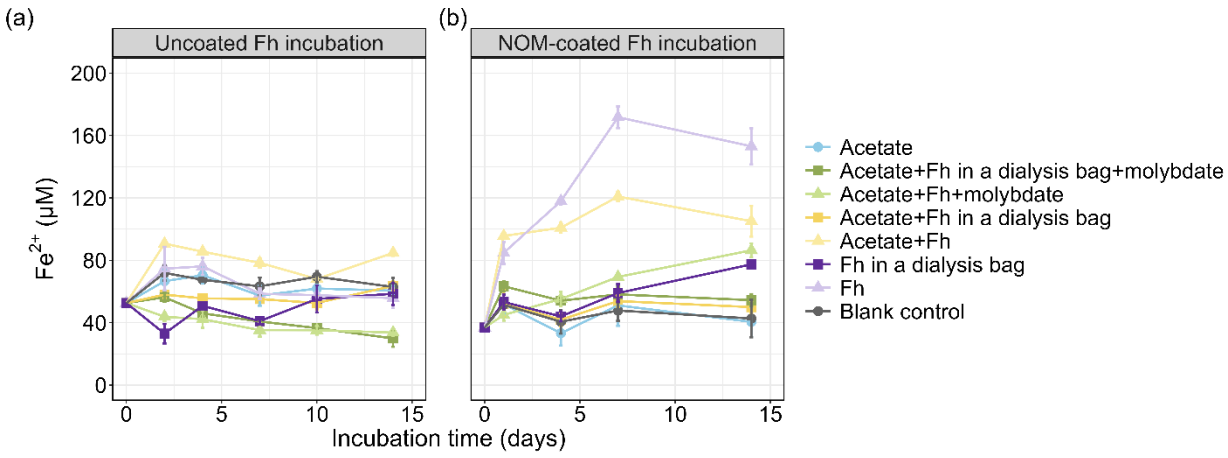

Figure 3. Fe^{2+} concentration in the supernatant of incubations with uncoated Fh (a) and NOM-coated Fh (b). Symbols indicate how Fh was added into the incubations: squares represent Fh placed in a dialysis bag, triangles represent Fh added directly in contact with the sediments, and circle represent treatments with no Fh. Mean Fe^{2+} concentrations are shown, and error bars represent the standard deviation of incubation triplicates (n = 3). Treatments with identical set-up, differing only in the status of Fh, are shown in paired lighter and darker colors. Fe^{2+} values in the treatments with molybdate do not represent true concentrations, as the ferrozine assay used for Fe^{2+} quantification is affected by the presence of molybdate[50] and yields overestimated values.

Addition of ferrihydrite slowed down the remineralization of ^{13}C-acetate

To quantify the amount of ^{13}C-acetate remineralized to dissolved inorganic carbon (DIC) during the 14-day incubation, we measured the $\delta^{13}C$ of DIC in the supernatant and calculated the remineralized ^{13}C-acetate using mass balance equations. In the uncoated Fh incubations, the ^{13}C-acetate concentration in the supernatant was 116 µM ± 11 µM at the beginning of the incubation, corresponding to ~10% of the maximum acetate adsorption capacity of the added Fh, as determined by the acetate adsorption experiment (Supplementary Figure 4). Therefore, the ^{13}C-acetate added could be adsorbed sufficiently by the added Fh. In absence of Fh protection, an average of 58 % of added ^{13}C-acetate was remineralized within 14 days, indicating the bio-availability of in-situ iron oxides in the Cumberland Bay sediments. With partial Fh protection allowing both biotic and abiotic iron reduction to remobilize Fh-associated ^{13}C-acetate, remineralization decreased to 44 %. With partial Fh protection allowing only abiotic iron reduction, 37 % of ^{13}C-acetate was remineralized, whereas allowing only biotic iron reduction resulted in 34 % remineralization. With full Fh protection allowing no iron reduction, remineralization was lowest, at 25 % (Figure 4, Supplementary Table 1).

Similar to the uncoated Fh incubations, in the NOM-coated Fh incubations, the ^{13}C-acetate concentration in the supernatant was 118 µM ± 1 µM at the beginning of the incubation. In absence of Fh protection, an average of 67 % of ^{13}C-acetate was remineralized within 14 days. With partial Fh protection allowing both biotic and abiotic iron reduction, 60 % of ^{13}C-acetate was remineralized. With partial Fh protection allowing only abiotic iron reduction, 55 % of ^{13}C-acetate was remineralized, whereas allowing only biotic iron reduction resulted in only 11 % remineralization. With full Fh protection inhibiting iron reduction, remineralization was lowest, only 6% (Figure 4, Supplementary Table 1).

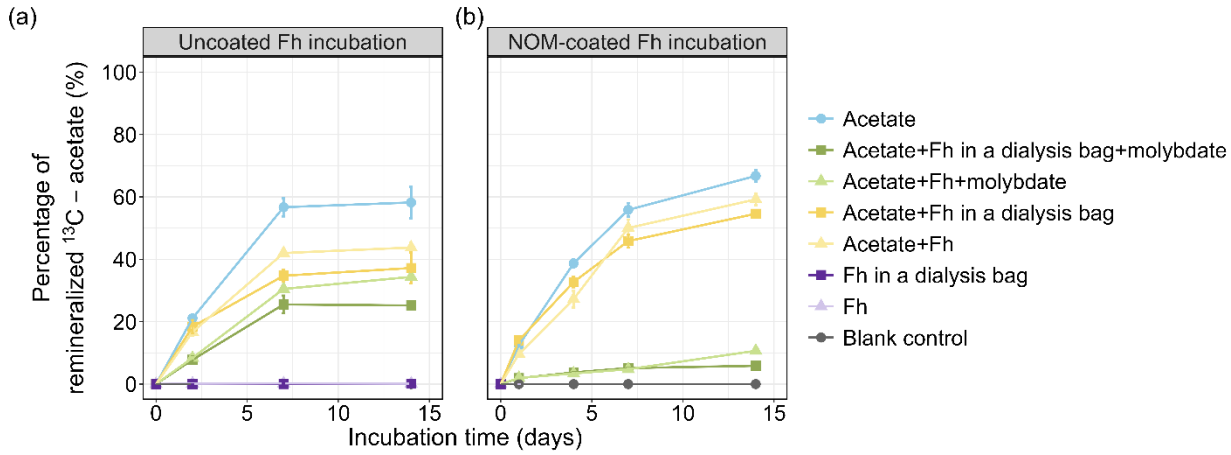

Figure 4. Percentage of ^{13}C-acetate remineralized to DIC in the supernatant during incubations with uncoated Fh (a) and NOM-coated Fh (b). Mean percentages of remineralized ^{13}C-acetate are shown, and error bars represent the standard deviation of incubation replicates (n = 3). Detailed concentrations of remineralized acetate are shown in Supplementary Table 1.

Thus, the addition of Fh, both uncoated and NOM-coated, slowed down the remineralization of ^{13}C-acetate. However, the observed Fh protection on acetate was apparently counteracted by microbially mediated iron reduction. Comparing the percentages of remineralized ^{13}C-acetate between full Fh protection and partial Fh protection that allowed biotic or abiotic iron reduction, it is evident that abiotic iron reduction played a more important role than biotic iron reduction in remobilizing Fh-associated ^{13}C-acetate, especially in the NOM-coated Fh incubations (Figure 4).

Considering relatively balanced iron and sulfate reduction in the incubation systems, abiotic iron reduction by sulfide seems to be more effective in remobilizing Fh-associated ^{13}C-acetate than iron-reducing microorganisms.

Given that the concentrations of iron oxide and acetate used in our incubation are within the range observed in natural settings, our results suggest that the presence of iron oxides can strongly influence the pool of acetate available to microorganisms in marine sediments and thus regulate the rate of acetate remineralization, a key terminal step in organic matter remineralization.

Ferrihydrite-associated ^{13}C-acetate could be remobilized by iron reduction

To further address how effectively Fh could protect acetate from degradation under microbial activities, all possible fates of acetate in the incubation systems were evaluated using samples collected on day 7. In total three fates were considered: (1) acetate was remineralized to DIC in the supernatant (scenario investigated above); (2) acetate remained in the supernatant as acetate; and (3) acetate was associated with solid phases, including Fh and sediment particles. There was also possibility that acetate was remineralized to CO_2 gas in the headspace, or, with a much smaller chance, turned into CH_4 gas through acetoclastic methanogenesis. However, the CO_2 and CH_4 concentrations in the headspace could only be translated to a ^{13}C-acetate concentration ranging from 0.1 μM to 1.1 μM, and therefore were not considered in the following evaluation (Supplementary Data 2).

To simplify the investigation, for treatments testing partial Fh protection, we selected the one with only abiotic iron reduction, as abiotic iron reduction had a much stronger effect in remobilizing Fh-associated acetate than biotic iron reduction (Figure 4). Apart from the concentration of ^{13}C-acetate being remineralized, the concentration of ^{13}C-acetate remaining in the supernatant (scenario 2) was determined as well. By

measuring the acetate concentration in the supernatant, the amount of ^{13}C-acetate was calculated using mass balance equations (See Methods for calculations). In uncoated Fh incubations, only when acetate was added together with Fh and molybdate, there was 9 % ± 1 % of ^{13}C-acetate left in the supernatant. Similarly, in NOM-coated Fh incubations, only when acetate was added together with Fh and molybdate, there was 6 % ± 1 % of ^{13}C-acetate left in the supernatant. In all the other treatments of both incubations, acetate remaining in the supernatant was below the detection limit, translating to a negligible amount of ^{13}C-acetate.

By subtracting the fractions of ^{13}C-acetate remineralized to DIC and remaining in the supernatant as acetate from the total ^{13}C-acetate budget, we calculated the fraction of ^{13}C-acetate associated with solid phases, such as Fh and sediment particles (scenario 3). The percentages of the three major fates of ^{13}C-acetate are shown in Figure 5. For the acetate associated with solid phases, results from the uncoated Fh incubations show that, in the absence of Fh protection, 43 % ± 3 % of the ^{13}C-acetate was associated with sediment particles, while under full Fh protection without microbial remobilization via abiotic iron reduction, 65 % ± 3 % of the acetate was associated with uncoated Fh and sediment particles. Therefore, adding uncoated Fh protected 51 % more ^{13}C-acetate. However, under partial Fh protection with microbial remobilization, 65 % ± 2 % of the ^{13}C-acetate remained associated, basically the same amount as under full Fh protection. This indicates that microbial processes played a very limited role in remobilizing Fh-associated ^{13}C-acetate when Fh was not coated with NOM (Figure 5a).

Interestingly, results from the NOM-coated Fh incubations were very different. In the absence of Fh protection, 44 % ± 2 % of the ^{13}C-acetate was associated with sediment particles, while under full Fh protection without microbial remobilization, 89 % ± 1 % of the ^{13}C-acetate was associated with NOM-coated Fh and sediment particles. This represents a 102 % increase in protected ^{13}C-acetate relative to the no-Fh condition. Compared with uncoated Fh, which protected only 51 % more ^{13}C-acetate, NOM-coated Fh was substantially more effective at protecting ^{13}C-acetate.

However, under partial Fh protection with microbial remobilization, only 54 % ± 2 % of the ^{13}C-acetate remained associated with NOM-coated Fh and sediment particles. This indicates that microbial processes remobilized approximately 77 % of the additional ^{13}C-acetate associated with NOM-coated Fh (Figure 5b).

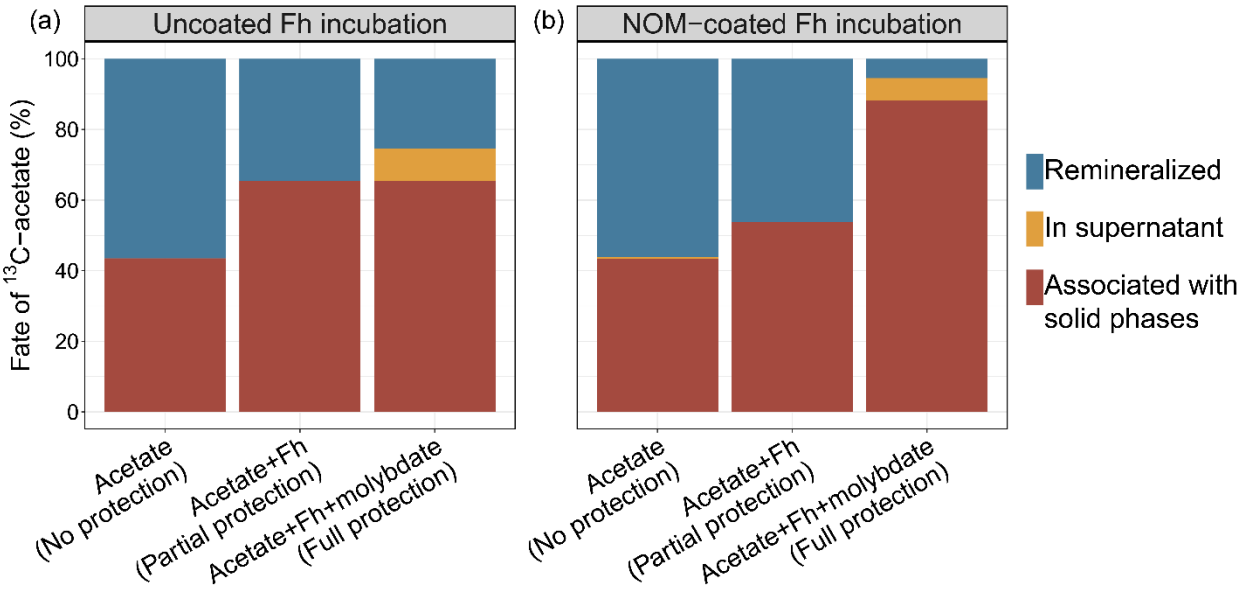

Figure 5. Fates of ^{13}C-acetate in uncoated and NOM-coated Fh incubations. In all the treatments shown here, Fh was first added into a dialysis bag before adding into the incubations to exclude most biotic iron reduction. Therefore, "Partial protection" here means partial Fh protection with abiotic iron reduction to remobilize Fh-associated ^{13}C-acetate. Bars show mean percentages of ^{13}C-acetate remineralized, remaining in the supernatant, and associated with solid phases. Data with error bars indicating the standard deviation of incubation replicates (n = 3) are shown in Supplementary Figure 8.

Results from the treatments without Fh protection show that minerals in the in-situ marine sediments, such as reactive iron oxides[49] and clay minerals, could adsorb a large part of ^{13}C-acetate. Although there was already no detectable ^{13}C-acetate in the supernatant in most of the treatments on day 7, more ^{13}C-acetate was remineralized from day 7 to day 14 (Figure 4). This suggested a dynamic adsorption and desorption of ^{13}C-acetate between liquid and solid phases. ^{13}C-acetate was detected only in the

supernatant of treatments with molybdate and Fh added in a dialysis bag, where there was no microbially mediated iron reduction to consistently remobilize acetate from the solid phases and no active sulfate reduction to remineralize acetate. The equilibrium between adsorption and desorption maintained the low concentrations of acetate in the supernatant. This provides strong evidence that microbial processes serve as a major driving force of the partitioning of acetate at the interface of sediment/iron oxide particles and pore water, and consequently regulate the acetate cycling.

Given that NOM in marine sediments exhibits an even stronger affinity than acetate for adsorption onto iron oxide surfaces (Supplementary Figure 3 and 4), the microbially mediated interaction between iron oxides and acetate we identified are likely not limited to the acetate molecule under laboratory conditions. Instead, microbial remobilization of NOM associated with iron oxides are expected to occur widely in natural marine sedimentary environments. This is potentially supported by the stimulation of iron reduction following the addition of NOM-coated Fh, indicating the NOM adsorbed on Fh may be remobilized and used by the microorganisms to drive iron reduction.

Natural organic matter coating changes the aggregation of iron oxides and their role in sedimentary carbon cycling

Comparing the fate of ^{13}C-acetate in uncoated and NOM-coated Fh incubations, the NOM coating strongly increased the capacity of Fh particles to adsorb acetate, while also enhancing the accessibility of Fh particles to microorganisms capable of remobilizing the adsorbed acetate. Previous studies have demonstrated that organic matter with a higher abundance of carboxyl groups adsorbs more extensively on Fh nanoparticles[31]. Subsequently, the aggregation of Fh nanoparticles was largely controlled by the molecular weight and the concentration of the adsorbed organic matter[31]. In particular, high concentrations of high-molecular-weight organic matter

can inhibit Fh aggregation due to steric repulsion[31]. In addition, goethite nanorods suspended in 50 ppm OC of Suwannee River humic acid had much smaller aggregate sizes resulting from steric and electrostatic repulsion[32]. The NOM extracted from marine sediments of Cumberland Bay, South Georgia, used here as a coating for Fh, has a similar chemical composition to Suwannee River humic acid, as both are rich in humic-like organic matter containing abundant carboxyl groups (Supplementary Figure 5). In our study, adsorption of NOM on iron oxides resulted in smaller aggregates as shown by SEM analysis of the uncoated and NOM-coated Fh (Figure 1). Smaller aggregates provide more surface area, which could explain the promoted interaction between NOM-coated Fh, organic molecules such as acetate and microorganisms.

In our incubation experiments, the treatments with partial Fh protection represents conditions characteristic of organic carbon-rich coastal sediments, where both biotic and abiotic iron reduction are occurring[11, 50]. Our observations suggest that, in such sedimentary environments, although NOM-coated iron oxides may provide large surface area to adsorb organic molecules from pore water, these adsorbed molecules remain readily accessible to microorganisms. In iron and sulfate reduction zones when both processes are coupled with the oxidation of buried organic matter, iron-reducing bacteria and sulfate-reducing bacteria are capable of reducing iron oxides[8, 9] (Figure 6). While within the sulfate-methane transition zone (SMTZ), where sulfate reduction is coupled with and stimulated by the oxidation of methane, hydrogen sulfide plays the major role in dissolving iron oxides[16, 17] and remobilizing iron-associated organic matter, as shown in our incubation experiments. In addition, anaerobic methanotrophic (ANME) archaea may be capable of coupling anaerobic oxidation of methane (AOM) directly with iron reduction and facilitate iron oxide dissolution in the SMTZ[10, 54, 55] (Figure 6). The increased accessibility of NOM-coated iron oxides could lead to stronger microbial remobilization of a substantial fraction of the adsorbed organic matter and offset the role of iron oxides in long-term carbon preservation (Figure 6).

The treatment with full Fh protection represents conditions characteristic of organic-poor pelagic sediments, where low sedimentation rates and limited OC input allow oxygen to penetrate the entire sediment column, covering 9 % - 37 % of the global seafloor[56]. In these persistently oxic sediments, iron reduction does not occur and therefore does not selectively remobilize iron-associated OC for remineralization. Compared to OC not associated with iron (non-iron-associated OC), iron-associated OC preserved within mineral mesopores has been hypothesized to be protected from enzymatic degradation (the “mesopore protection hypothesis”) [57]. Meanwhile, iron-associated OC with more functional groups binding with iron oxides becomes increasingly stabilized as the iron oxides age and transform into more crystalline forms[58]. Highly crystalline iron oxides have been shown to be largely associated with pre-aged terrestrial OC, suggesting a potential coupled maturation process between iron and iron-associated OC[59]. OC persisting over millions of years has been found in the oligotrophic North Atlantic and South Pacific, where proteinaceous OC is protected by adsorption to mineral surfaces[60]. As a result, iron-associated OC may be better preserved than non-iron-associated OC during burial under prolonged oxic conditions, contributing an increasingly important carbon pool in deeper sediments. In these sedimentary environments, NOM-coated iron oxides likely further promote the carbon preservation in long buried sediments (Figure 6).

Therefore, natural organic matter coatings fundamentally reshape the role of iron oxides in protecting organic carbon in marine sediments. NOM-coated iron oxides function as dynamic interfaces that simultaneously enhance organic carbon preservation and facilitate microbial remobilization, especially in organic-rich sediments with active microbially mediated iron reduction. This challenges the traditional view of iron oxides protecting organic carbon from degradation through adsorption, which may only apply for oxic marine sediments. Recognizing this dual functionality is critical in understanding how iron oxides may alter the balance between carbon sequestration and remineralization in various marine environments.

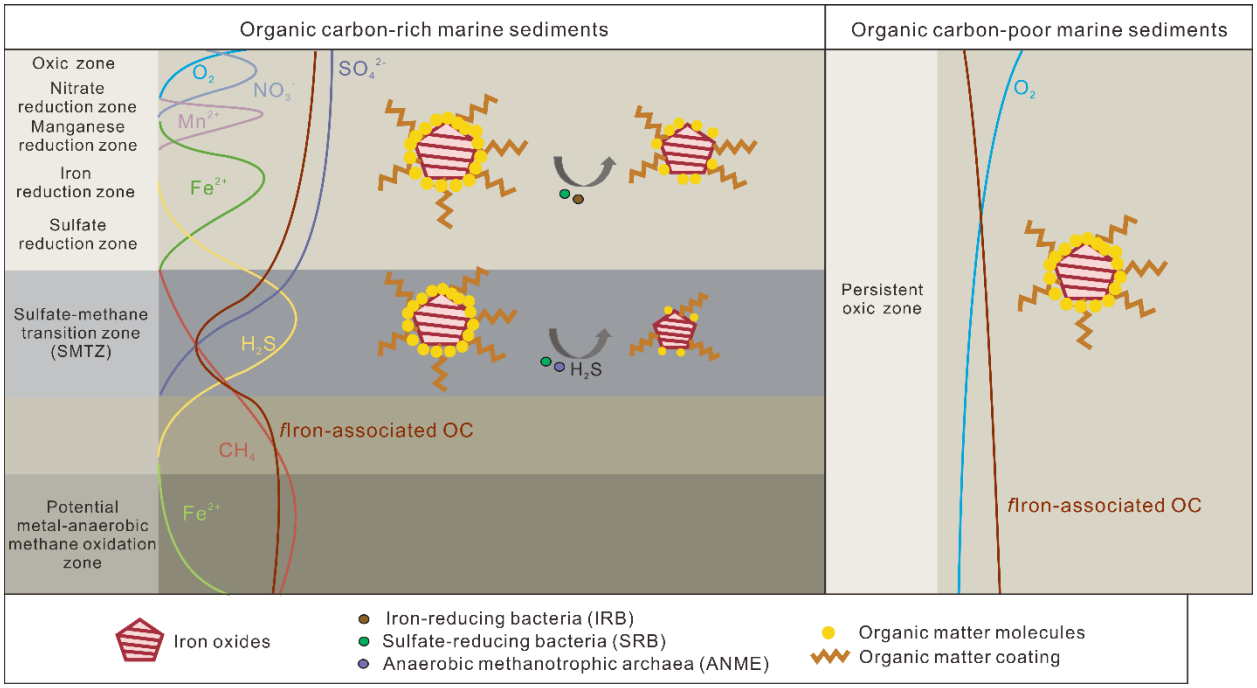

Figure 6. Schematic suggesting how natural organic matter coating on iron oxides may contribute differently in carbon preservation in organic-rich and -poor marine sediments. "*f*Iron-associated OC" represents the fraction of iron-associated OC in total organic carbon.

Materials and Methods

Study area and sampling

Sediments around South Georgia were collected during the expedition PS133-2 "Island Impact" of RV *Polarstern* in November and December 2022[38], where >90% of its glaciers have retreated since the 1950s[61]. The glacial meltwater supplies iron to the bay area[62], which made it an ideal area to study the interaction between iron-containing minerals and organic matter.

Surface sediments were retrieved using a multicorer (MUC). The sediments were preserved in 250 mL Schott bottles with limited headspace filled with N_2, sealed with rubber stoppers, and preserved anoxically at 2 °C until use. Sediments from Confluence Zone, outer Cumberland Bay (MUC core PS133-2-42-9-4, 4-12 cmbsf,

54°12.521' S, 36°26.514' W) were used in this study for both adsorption experiments and incubation experiments. General sediment properties, including porewater geochemistry, sulfate reduction rates, reactive iron oxide content, TOC content, and sedimentation rates, were described by Ebner et al. (2026) [49].

Adsorption experiments with ferrihydrite

Two-line ferrihydrite (Fh) was synthesized according to the method of Schwertmann and Cornell[63]. Briefly, KOH solution was added into $Fe(NO_3)_3 \cdot 9H_2O$ solution dropwise until the pH reached 7.5 while stirring vigorously. Then, Fh slurry was transferred to centrifuge tubes and centrifuged at 3000 *g* for 10 min to remove the supernatant. Fh particles were washed 5 times with Milli-Q water to remove salts. After washing, Fh particles were resuspended in Milli-Q water and kept as a stock slurry at 4 °C for further use.

Freeze-dried sediments were grinded, mixed with Milli-Q water in a ratio of 1:6 (w:v), and shaken at 200 rpm at 20 °C for 24 h. The supernatant was collected by a 10 min centrifugation at 3000 *g* and filtered through a 0.7 µm glass fiber membrane (combusted at 450 °C for 5 h) and a 0.22 µm polycarbonate membrane (rinsed with Milli-Q water) to remove sediment particles and microorganisms. The water-extractable organic matter solution was used as natural organic matter (NOM) solution in the adsorption experiment.

To prepare NOM-coated Fh, 1 mmol Fh was mixed with 40 mL of NOM solution in each tube and shaken at 100 rpm at 20 °C for 72 h. 40 mL of NOM solution was shaken without Fh and served as a blank control to check NOM adsorption onto the tube. Three replicates were sacrificed for dissolved organic carbon (DOC) analysis using a carbon analyzer (Multi N/C 2100S, Analytic Jena) every 24 h to track the adsorption of NOM. No adsorption of NOM on the tube was observed. Therefore, the amount of NOM adsorbed on Fh was determined as the difference in DOC concentration in the supernatant before and after the adsorption. After the NOM adsorption experiment, the solids were collected, rinsed once with Milli-Q water to

remove traces from NOM solution and stored as moist solids under 4 °C. The moist solids were resuspended in artificial sea water (ASW, 26 g NaCl, 5 g $MgCl_2 \cdot 6\ H_2O$, 1.4 g $CaCl_2 \cdot 2H_2O$, 9.1 g $Na_2SO_4 \cdot 10H_2O$, 0.3 g NH_4Cl, 0.1 g KH_2PO_4, 0.5 g KCl filled up with Milli-Q water to 1 L) on the next day before setting up the incubation and used as NOM-coated Fh in the incubations.

To evaluate the ability of Fh to protect acetate from microbial degradation during subsequent incubations with marine sediments, the amount of ^{13}C-acetate was added at a concentration that could be fully adsorbed by the Fh added. Therefore, the adsorption efficiency of acetate on Fh was determined following the same procedure used for NOM. 40 mL of the acetate solution with a concentration of 1.71 mM was mixed with 0.5 mmol of Fh in each tube and shaken at 100 rpm at 20 °C for 24 h. 40 mL of acetate solution was shaken without Fh and served as a blank control to check acetate adsorption onto the tube. All the treatments were performed in triplicates. Concentrations and carbon isotopic compositions of acetate in the supernatant were analyzed by isotope-ratio-monitoring liquid chromatography/mass spectrometry (irm-LC/MS) as described in a previous study[47] using a Thermo Scientific™ Dionex UltiMate 3000 HPLC system that is coupled via LC IsoLink™ interface (also from Thermo Scientific™) to a ThermoFinnigan Delta Plus XP isotope ratio mass spectrometer. Adsorption of acetate on the tubes was observed. Therefore, the acetate adsorbed on Fh was determined as the difference in acetate concentration between treatments with and without Fh after 24 h of adsorption.

Characterization of NOM optical properties

Optical properties of fluorescent dissolved organic matter (FDOM) in NOM solution before and after the adsorption experiment were characterized by 3D excitation emission matrix (EEM) fluorescence measurement using a 3D fluorescence spectrometer (Cary Eclipse, Agilent Technologies). Fluorescence EEMs were collected over excitation wavelengths ranging from 230 nm to 500 nm at 5 nm intervals and emission wavelengths ranging from 250 nm to 550 nm at 2 nm intervals, with an integration time of 1 s. UV-Vis absorbance spectra were collected

from 220 nm to 700 nm to correct the inner-filter effect in EEMs. Milli-Q water served as blanks during the measurements. Before optical indices calculation, blanks were subtracted, scatters were removed, inner-filter effects were corrected, and fluorescence data were converted to Raman units (R.U.) by normalizing the fluorescence collected in arbitrary units to the Raman peak area at excitation 350 nm[64]. Optical indices humification index (HIX) was calculated as the area under the emission spectra 435 nm − 480 nm divided by the area under 300 nm − 345 nm and 435 nm − 480 nm at the excitation wavelength 254 nm, which represents the extent of humification[65]. Both data correction and indices calculation were performed in R (version 4.3.2) using the staRdom package[66].

Structural characterization of Fh particles

To compare the average crystallite sizes (ACS) of the uncoated Fh, NOM- and acetate-coated Fh, laboratory total scattering experiments were carried out using Ge(111) monochromatized Mo-radiation (0.070293 nm) on a StadiMP diffractometer (Stoe, Darmstadt) in Debye-Scherrer-geometry. Freeze dried samples were prepared in 0.5 mm capillaries (G50, Hilgenberg) and measured for 5 days. Data reduction and calculation of the G(r) was carried out using GudrunX (S.E. McLain et al. 2006) and measurement data from an empty capillary. The G(r) of the samples were analyzed using the EnvACS procedure[67], using the envelope function by Howell et al. [68], enabling the determination of the ACS as well as its distribution.

To assess whether Fh aggregation is altered by NOM coating or incubation with acetate, uncoated Fh and NOM-coated Fh were incubated with an acetate solution (100 µM), similar to the concentration of ^{13}C-acetate used in the sediment incubations, for 2 weeks. Uncoated and NOM-coated Fh, both with and without incubation with acetate, were split into 3 triplicates using a rotary suspension splitter. The particle size distribution analysis was performed with a Beckman Coulter Laser Diffraction Particle Size Analyzer LS 13320. The obtained results provided the particle-size distribution of a sample from 0.04 µm to 2000 µm. The reproducibility was checked regularly by replicate analyses of three internal glass-bead standards

and was found to be better than ±0.7 μm for the mean and ± 0.6 μm for the median particle size (1σ).

The uncoated and NOM-coated Fh, both with and without incubation with acetate solution, were freeze dried and their morphology and elemental distribution were visualized using a field emission scanning electron microscope (FESEM; SUPRA 40, Zeiss) coupled to an energy-dispersive X-ray spectroscopy (EDS) detector (XFlash 6-30, Bruker).

Incubation set-up

Anoxic sediment slurries were prepared at a ratio of 1:2 (w:v) of wet sediment and artificial seawater (26 g NaCl, 5 g $MgCl_2 \cdot 6\ H_2O$, 1.4 g $CaCl_2 \cdot 2H_2O$, 9.1 g $Na_2SO_4 \cdot 10H_2O$, 0.3 g NH_4Cl, 0.1 g KH_2PO_4, 0.5 g KCl filled up with Milli-Q water to 1 L) and 50 mL were distributed into each 120 mL serum bottle in anaerobic chamber filled with pure N_2 gas (UNIlab SP, MBRAUN, Germany). The serum bottles were sealed with butyl rubber stoppers and crimped with aluminum caps. To ensure the depletion of alternative electron acceptors (e.g., nitrate) potentially present in the starting sediments, slurries were pre-incubated at 5 °C in the dark for 2 weeks before the addition of substrates. Following the pre-incubation, eight different treatments were set up in triplicates to study the degradation of ^{13}C-acetate under the protection by Fh (Table 1).

Table 1. Incubation set-up[a]

Treatment (n = 3)	^{13}C-acetate[b] (120 µM)	Ferrihydrite[c] (20 mM)	Molybdate[d] (28 mM)	Purpose, tracking
Acetate	X			acetate degradation without Fh protection
Acetate+Fh +molybdate	X	X (In a dialysis bag)	X	acetate degradation with full Fh protection
Acetate+Fh +molybdate	X	X	X	acetate degradation with partial Fh protection allowing biotic iron reduction
Acetate+Fh	X	X (In a dialysis bag)		acetate degradation with partial Fh protection allowing abiotic iron reduction
Acetate+Fh	X	X		acetate degradation with partial Fh protection allowing biotic and abiotic iron reduction
Fh		X (In a dialysis bag)		abiotic reduction of Fh
Fh		X		biotic and abiotic reduction of Fh

Blank control	background biotic and abiotic iron reduction

Note:

[a] The incubations were performed in parallel using uncoated Fh and NOM-coated Fh, respectively; both are denoted as “Fh” in the table.

[b] For all treatments with acetate, parallel incubations (n = 3) were set up with unlabeled acetate to measure acetate concentration and carbon isotope ratios. Its carbon isotope ratio differs sufficiently from that of acetate produced during organic matter degradation, while not being overly enriched for the instrument. These incubations were used solely to estimate the amount of ^{13}C-acetate remaining in the supernatant and were therefore not listed as separate treatments in the table.

[c] In some treatments, Fh slurry resuspended in ASW was added into Spectra/Por ® 4 Dialysis membrane bags with a molecular weight cut-off of 12-14 kDa (Spectrum Laboratories, Inc.). In this case, most biotic iron reduction requiring direct contact with the iron mineral surface were assumed to be excluded, while acetate and biogenetic sulfide by the sulfate reducers were still able to diffuse into the dialysis bag and reduce Fh abiotically.

[d]Molybdate was added to inhibit the microbial reduction of sulfate to sulfide, and thereby abolishing abiotic iron reduction through sulfide as reductant.

Geochemical measurements

During the incubation, slurry samples were taken anoxically and the solid phase was separated from the supernatant by a 5 min centrifugation at 12,100 *g*. Solid samples for geochemical analyses were preserved at -20 °C. Supernatant samples for Fe^{2+} analysis were preserved with HCl (0.5 M final concentration), and samples for sulfide analysis were fixed with zinc acetate (2.5 % w/v final concentration). Concentrations of iron and sulfide were determined photometrically using the ferrozine[69] and Cline[70] assays, respectively, with a microplate reader (VANTAstar, BMG Labtech).

The method for dissolved inorganic carbon (DIC) analysis has been reported elsewhere[71]. Briefly, supernatant samples were filtered through a 0.2 µm filter to remove particles and an aliquot of 1 mL was acidified with 100 µL of 45 % phosphoric acid overnight in an Exetainer vial, pre-purged with CO_2-free air before analysis. DIC concentration and its carbon isotope ratio were measured using a Delta Ray isotope ratio infrared spectrometer with universal reference interface and Cetac ASX-7100 autosampler (Thermo Fisher Scientific, Bremen). The isotopic values were reported in the delta notation as $\delta^{13}C$ relative to the VPDB standard with a precision of < 3 % (standard deviation). DIC concentration was calculated from the detected total volume of CO_2 in the Exetainer vial headspace by a calibration series prepared with sodium bicarbonate solution.

The method for acetate measurement has been published previously[45]. Briefly, the samples were filtered through a 0.2 µm filter to remove all the particles. The acetate concentration and its carbon isotope ratio were determined using a high-performance liquid chromatography (Surveyor, Thermo Finnigan) coupled to a continuous-flow irm-MS (Delta Plus XP, Thermo Finnigan), via a Finnigan™ LC IsoLink interface. The detection limit for acetate concentration was 9 µM, with a precision of 0.8 %. The precision of acetate carbon isotope measurement was 1.0 %. Precision was determined as the relative standard deviation of repeated measurements of the standard.

Calculation of the carbon isotope ratio of ^{13}C-acetate

The ^{13}C-acetate used in the incubation was prepared by mixing unlabeled, i.e., natural isotopic, acetate and 99% labeled acetate with the same concentration at a ratio of 9:1. The R value ($^{13}C/^{12}C$) of ^{13}C-acetate was calculated as follows:

$$R_{13_{C-acetate}} = \frac{n_{99\%-\text{labeled}} \times f^{13}C_{99\%-\text{labeled}} + n_{\text{unlabeled}} \times f^{13}C_{\text{unlabeled}}}{n_{99\%-\text{labeled}} \times f^{12}C_{99\%-\text{labeled}} + n_{\text{unlabeled}} \times f^{12}C_{\text{unlabeled}}},$$

where *n* is defined as the amount of acetate in mol;

$f^{13}C$ is defined as the relative percentage of ^{13}C, which can be calculated from the R value:

$f^{13}C = {}^{13}C/({}^{13}C+{}^{12}C) = R/(R+1)$;

$f^{12}C = 1- f^{13}C$

The carbon isotope ratio of ^{13}C-acetate was calculated in the delta notation as $\delta^{13}C$ relative to the VPDB standard to be 9890‰.

Quantification of acetate remineralized to DIC

The DIC in the incubation system was assumed to come from two major sources, one was the DIC produced during the remineralization of ^{13}C-acetate (DIC_acetate) and the other was the DIC produced during the remineralization of indigenous organic matter in the sediments (DIC_sedi). The relative contribution of DIC from these two sources could be calculated based on a mass balance equation:

$\delta^{13}C_{DIC} = \delta^{13}C_{DIC\_acetate} \times f_{DIC\_acetate} + \delta^{13}C_{DIC\_sedi} \times f_{DIC\_sedi}$

$f_{DIC\_acetate} + f_{DIC\_sedi} = 1$,

where

$\delta^{13}C_{DIC}$ was the measured carbon isotope ratio of DIC in the supernatant;

the carbon isotope ratio of ^{13}C-acetate (9890‰) was taken for $\delta^{13}C_{DIC\_acetate}$;

the measured carbon isotope ratio in the supernatant of blank control group was taken for $\delta^{13}C_{DIC\_sedi}$;

$f_{DIC\_acetate}$ represents the fraction of DIC produced by the remineralization of ^{13}C-acetate in the total DIC pool in the supernatant;

f_{DIC_sedi} represents the fraction of DIC produced by the remineralization of organic carbon from sediments in the supernatant.

Quantification of acetate remaining in supernatant

Similar to DIC, the acetate in the supernatant of the incubation system was assumed to come from two major sources. One was the acetate added as substrates (acetate_chem) and the other was the acetate produced during the degradation of indigenous organic matter in the sediments (acetate_sedi). The parallel incubations amended with unlabeled acetate were used for acetate quantification; its carbon isotope ratio differs sufficiently from that of acetate produced during organic matter degradation, while not being overly enriched for the instrument. The relative contribution of acetate from these two sources could be calculated based on a mass balance equation:

$$\delta^{13}C_{acetate} = \delta^{13}C_{acetate\_chem} * f_{acetate\_chem} + \delta^{13}C_{acetate\_sedi} * f_{acetate\_sedi}$$

$$f_{acetate\_chem} + f_{acetate\_sedi} = 1,$$

where

$\delta^{13}C_{acetate}$ is the measured carbon isotope ratio of acetate in the supernatant;

$\delta^{13}C_{acetate\_chem}$ is carbon isotope ratio of unlabeled chemical of sodium acetate;

the measured carbon isotope ratio in the supernatant of blank control group was taken for $\delta^{13}C_{acetate\_sedi}$;

$f_{acetate\_chem}$ represents the fraction of added acetate chemical in the total acetate pool in the supernatant;

$f_{acetate\_sedi}$ represents the fraction of acetate coming from natural sediments in the total acetate pool in the supernatant.

Headspace measurement

Gas samples (100 µL) were taken from the headspace of the serum bottles at different time points using a gas tight syringe. Concentrations of CH_4 and CO_2 were measured using the Shimadzu GC 2014 gas chromatography system equipped with a Porapak Q column (length, 2 m; inner diameter, 2 mm), a Methanizer

(Varian/Agilent, CP11952), and a flame ionization detector. The CO_2 gas was transformed to CH_4 by the Methanizer to become detectable and then detected. The column, Methanizer and detector temperatures were set to 70 °C, 350 °C and 200 °C, respectively. The carrier gas was hydrogen (99.999%) at a flow rate of 30 mL min^{-1}. Different volumes of a standard gas with 1000 ppmV of both CO_2 and CH_4 were measured for quantification before the samples.

Acknowledgements

We thank the crew and scientific party of RV *Polarstern* during cruise PS133-2 for supporting sample collection. We thank Dr. Jürgen Titschack from University of Bremen for the help with particle size analysis and Petra Witte from University of Bremen for the help with FESEM-EDS analysis. This work was funded by the German Research Foundation (DFG) under Germany's Excellence Strategy (EXC-2077-390741603). Funding for expedition PS133 was provided by the Helmholtz Association (Alfred Wegener Institute Helmholtz Centre for Polar and Marine Research) in the framework of the Helmholtz Research Program "Changing Earth – Sustaining our Future" in PoF IV. Data of the cruise PS133-2 were collected under Grant No. AWI_PS133/2_1.

Author contributions

Conceptualization: Yunru Chen, Matthias Zabel, Kai-Uwe Hinrichs, Michael W. Friedrich

Methodology: Yunru Chen, Heidi Taubner, Verena Heuer, Lars Robben, Wolfgang Bach

Sample acquisition: Lea C. Wunder, Graciana Willis-Poratti, Sabine Kasten

Investigation: Yunru Chen, Heidi Taubner, Verena Heuer, Jenny Altun, Rianne van Kaam, Lars Robben, Wolfgang Bach, Anna Helms

Data curation: Yunru Chen, Heidi Taubner, Verena Heuer, Jenny Altun, Rianne van Kaam, Lars Robben, Wolfgang Bach

Visualization: Yunru Chen

Writing – original draft: Yunru Chen

Writing – review & editing: Yunru Chen, Heidi Taubner, Verena Heuer, Jenny Altun, Rianne van Kaam, Lars Robben, Wolfgang Bach, Lea C. Wunder, Graciana Willis-Poratti, Sabine Kasten, Matthias Zabel, Kai-Uwe Hinrichs, Michael W. Friedrich

Funding acquisition: Sabine Kasten, Matthias Zabel, Kai-Uwe Hinrichs, Michael W. Friedrich

Competing interests

The authors declare that they have no competing interests.

Data availability

All data discussed in this paper are available in the Supplementary Data and the Source data file, which are provided with this paper and also available in the Figshare database (10.6084/m9.figshare.31956066).

References

1. Berner RA. GEOCARBSULF: A combined model for Phanerozoic atmospheric O2 and CO2. *Geochim Cosmochim Acta* 70, 5653-5664 (2006), https://doi.org/10.1016/j.gca.2005.11.032.
2. Longman J, Faust JC, Bryce C*, et al.* Organic carbon burial with reactive iron across global environments. *Global Biogeochemical Cycles* 36, e2022GB007447 (2022), https://doi.org/10.1029/2022GB007447.

3. Jones D, Edwards A. Influence of sorption on the biological utilization of two simple carbon substrates. *Soil Biol Biochem* 30, 1895-1902 (1998), https://doi.org/10.1016/S0038-0717(98)00060-1.
4. Adhikari D, Dunham-Cheatham SM, Wordofa DN*, et al.* Aerobic respiration of mineral-bound organic carbon in a soil. *Sci Total Environ* 651, 1253-1260 (2019),
5. Eusterhues K, Neidhardt J, Hädrich A*, et al.* Biodegradation of ferrihydrite-associated organic matter. *Biogeochemistry* 119, 45-50 (2014),
6. Melton ED, Swanner ED, Behrens S*, et al.* The interplay of microbially mediated and abiotic reactions in the biogeochemical Fe cycle. *Nat Rev Microbiol* 12, 797–808 (2014), https://doi.org/10.1038/nrmicro3347.
7. Liang L, Vigderovich H, Sivan O*, et al.* Iron (oxyhydr)oxides shift the methanogenic community in deep sea methanic sediment - insights from long-term high-pressure incubations. *Sci Total Environ* 848, 157590 (2022), https://doi.org/10.1016/j.scitotenv.2022.157590.
8. Lovley DR, Roden EE, Phillips EJP*, et al.* Enzymatic iron and uranium reduction by sulfate-reducing bacteria. *Mar Geol* 113, 41-53 (1993), https://doi.org/10.1016/0025-3227(93)90148-O.
9. Lovley DR, Phillips EJ. Novel mode of microbial energy metabolism: organic carbon oxidation coupled to dissimilatory reduction of iron or manganese. *Appl Environ Microbiol* 54, 1472-1480 (1988), https://doi.org/10.1128/aem.54.6.1472-1480.1988.
10. Aromokeye DA, Kulkarni AC, Elvert M*, et al.* Rates and microbial players of iron-driven anaerobic oxidation of methane in methanic marine sediments. *Front Microbiol* 10, 3041 (2020),
11. Müller D, Liu B, Holtappels M*, et al.* Rates and pathways of organic matter remineralisation in different sedimentary environments of the Helgoland Mud Area, North Sea. *Cont Shelf Res* 298, 105632 (2026), https://doi.org/10.1016/j.csr.2025.105632.

12. Henkel S, Kasten S, Poulton SW*, et al.* Determination of the stable iron isotopic composition of sequentially leached iron phases in marine sediments. *Chem Geol* 421, 93-102 (2016), https://doi.org/10.1016/j.chemgeo.2015.12.003.
13. Baloza M, Henkel S, Geibert W*, et al.* Benthic Carbon Remineralization and Iron Cycling in Relation to Sea Ice Cover Along the Eastern Continental Shelf of the Antarctic Peninsula. *J Geophys Res Oceans* 127, e2021JC018401 (2022), https://doi.org/10.1029/2021JC018401.
14. Baloza M, Henkel S, Kasten S*, et al.* The Impact of Sea Ice Cover on Microbial Communities in Antarctic Shelf Sediments. *Microorganisms* 11, 1572 (2023),
15. Poulton SW, Krom MD, Raiswell R. A revised scheme for the reactivity of iron (oxyhydr) oxide minerals towards dissolved sulfide. *Geochim Cosmochim Acta* 68, 3703-3715 (2004), https://doi.org/10.1016/j.gca.2004.03.012.
16. Riedinger N, Brunner B, Krastel S*, et al.* Sulfur Cycling in an Iron Oxide-Dominated, Dynamic Marine Depositional System: The Argentine Continental Margin. *Frontiers in Earth Science* Volume 5 - 2017, (2017), 10.3389/feart.2017.00033.
17. Riedinger N, Pfeifer K, Kasten S*, et al.* Diagenetic alteration of magnetic signals by anaerobic oxidation of methane related to a change in sedimentation rate. *Geochim Cosmochim Acta* 69, 4117-4126 (2005),
18. Chen Y, Dong L, Sui W*, et al.* Cycling and persistence of iron-bound organic carbon in subseafloor sediments. *Nat Commun* 15, 6370 (2024), https://doi.org/10.1038/s41467-024-50578-5.
19. Hu Y, Li K, Faust JC*, et al.* Stability of Reactive Iron-Bound Organic Carbon During Sulfidization of Iron Oxides: Insights From Methane-Seep Sediments. *Geophys Res Lett* 52, e2024GL112119 (2025), https://doi.org/10.1029/2024GL112119.

20. Zhao B, Fu L, Yao P*, et al.* Enhanced preservation of dark organic carbon by reactive iron in cold-seep sediments. *Chem Geol* 695, 123078 (2025), https://doi.org/10.1016/j.chemgeo.2025.123078.
21. Ye W, Chen Y, Yang C*, et al.* Dynamics of Iron-Bound Organic Carbon Across Different Development Stages of Marine Cold Seeps. *Global Biogeochemical Cycles* 40, e2025GB008889 (2026), https://doi.org/10.1029/2025GB008889.
22. Raiswell R. Iron Transport from the Continents to the Open Ocean: The Aging–Rejuvenation Cycle. *Elements* 7, 101-106 (2011), 10.2113/gselements.7.2.101.
23. Kaiser K, Mikutta R, Guggenberger G. Increased stability of organic matter sorbed to ferrihydrite and goethite on aging. *Soil Sci Soc Am J* 71, 711-719 (2007),
24. Han L, Sun K, Keiluweit M*, et al.* Mobilization of ferrihydrite-associated organic carbon during Fe reduction: Adsorption versus coprecipitation. *Chem Geol* 503, 61-68 (2019),
25. Eusterhues K, Hädrich A, Neidhardt J*, et al.* Reduction of ferrihydrite with adsorbed and coprecipitated organic matter: microbial reduction by Geobacter bremensis vs. abiotic reduction by Na-dithionite. *Biogeosciences* 11, 4953-4966 (2014), 10.5194/bg-11-4953-2014.
26. Cooper RE, Eusterhues K, Wegner C-E*, et al.* Ferrihydrite-associated organic matter (OM) stimulates reduction by Shewanella oneidensis MR-1 and a complex microbial consortia. *Biogeosciences* 14, (2017),
27. Adhikari D, Zhao Q, Das K*, et al.* Dynamics of ferrihydrite-bound organic carbon during microbial Fe reduction. *Geochim Cosmochim Acta* 212, 221-233 (2017),
28. Kleber M, Bourg IC, Coward EK*, et al.* Dynamic interactions at the mineral–organic matter interface. *Nature Reviews Earth & Environment* 2, 402-421 (2021), https://doi.org/10.1038/s43017-021-00162-y.

29. Kleber M, Eusterhues K, Keiluweit M*, et al.* Mineral–organic associations: formation, properties, and relevance in soil environments. In: *Advances in agronomy*). Elsevier (2015).
30. Liu J, Louie SM, Pham C*, et al.* Aggregation of ferrihydrite nanoparticles: Effects of pH, electrolytes,and organics. *Environ Res* 172, 552-560 (2019), https://doi.org/10.1016/j.envres.2019.03.008.
31. Li Z, Louie SM, Zhao J*, et al.* Deciphering the Roles of Molecular Weight and Carboxyl Richness of Organic Matter on Their Adsorption onto Ferrihydrite Nanoparticles and the Resulting Aggregation. *Environ Sci Technol* 58, 20480-20489 (2024), 10.1021/acs.est.4c06885.
32. Vindedahl AM, Strehlau JH, Arnold WA*, et al.* Organic matter and iron oxide nanoparticles: aggregation, interactions, and reactivity. *Environmental Science: Nano* 3, 494-505 (2016), 10.1039/C5EN00215J.
33. Heuer V, Krüger M, Elvert M*, et al.* Experimental studies on the stable carbon isotope biogeochemistry of acetate in lake sediments. *Org Geochem* 41, 22-30 (2010), 10.1016/j.orggeochem.2009.07.004.
34. Sørensen J, Christensen D, Jørgensen BB. Volatile Fatty Acids and Hydrogen as Substrates for Sulfate-Reducing Bacteria in Anaerobic Marine Sediment. *Appl Environ Microbiol* 42, 5-11 (1981), doi:10.1128/aem.42.1.5-11.1981.
35. Sansone FJ, Martens CS. Volatile fatty acid cycling in organic-rich marine sediments. *Geochim Cosmochim Acta* 46, 1575-1589 (1982), https://doi.org/10.1016/0016-7037(82)90315-5.
36. Carta D, Casula MF, Corrias A*, et al.* Structural and magnetic characterization of synthetic ferrihydrite nanoparticles. *Materials Chemistry and Physics* 113, 349-355 (2009), https://doi.org/10.1016/j.matchemphys.2008.07.122.
37. Michel FM, Ehm L, Antao SM*, et al.* The Structure of Ferrihydrite, a Nanocrystalline Material. *Science* 316, 1726-1729 (2007), doi:10.1126/science.1142525.

38. Kasten S. The Expedition PS133/2 of the Research Vessel POLARSTERN to the Scotia Sea in 2022. In: *Berichte zur Polar- und Meeresforschung = Reports on polar and marine research* (editors Bornemann H, Amir Sawadkuhi S). Alfred-Wegener-Institut Helmholtz-Zentrum für Polar- und Meeresforschung (2023).
39. Wagai R, Mayer LM. Sorptive stabilization of organic matter in soils by hydrous iron oxides. *Geochim Cosmochim Acta* 71, 25-35 (2007),
40. Villacís-García M, Ugalde-Arzate M, Vaca-Escobar K*, et al.* Laboratory synthesis of goethite and ferrihydrite of controlled particle sizes. *Boletín de la Sociedad Geológica Mexicana* 67, 433-446 (2015),
41. Huang X, Liang Y, Ye Q*, et al.* Theoretical modeling of molecular fractionation of dissolved organic matter on ferrihydrite and its impact on proton and metal binding properties. *Sci Total Environ* 888, 164276 (2023), https://doi.org/10.1016/j.scitotenv.2023.164276.
42. Lv J, Zhang S, Wang S*, et al.* Molecular-scale investigation with ESI-FT-ICR-MS on fractionation of dissolved organic matter induced by adsorption on iron oxyhydroxides. *Environ Sci Technol* 50, 2328-2336 (2016),
43. Sowers TD, Holden KL, Coward EK*, et al.* Dissolved Organic Matter Sorption and Molecular Fractionation by Naturally Occurring Bacteriogenic Iron (Oxyhydr) oxides. *Environ Sci Technol* 53, 4295-4304 (2019),
44. Heuer V, Inagaki F, Morono Y*, et al.* Temperature limits to deep subseafloor life in the Nankai Trough subduction zone. *Science* 370, 1230-1234 (2020), https://doi.org/10.1126/science.abd7934.
45. Heuer VB, Pohlman JW, Torres ME*, et al.* The stable carbon isotope biogeochemistry of acetate and other dissolved carbon species in deep subseafloor sediments at the northern Cascadia Margin. *Geochim Cosmochim Acta* 73, 3323-3336 (2009), https://doi.org/10.1016/j.gca.2009.03.001.

46. King GM. Measurement of Acetate Concentrations in Marine Pore Waters by Using an Enzymatic Approach. *Appl Environ Microbiol* 57, 3476-3481 (1991), doi:10.1128/aem.57.12.3476-3481.1991.

47. Heuer V, Elvert M, Tille S*, et al.* Online delta C-13 analysis of volatile fatty acids in sediment/porewater systems by liquid chromatography-isotope ratio mass spectrometry. 4, 346-357 (2006), https://doi.org/10.4319/lom.2006.4.346.

48. Glombitza C, Egger M, Røy H*, et al.* Controls on volatile fatty acid concentrations in marine sediments (Baltic Sea). *Geochim Cosmochim Acta* 258, 226-241 (2019), https://doi.org/10.1016/j.gca.2019.05.038.

49. Ebner B, Henkel S, Kraal P*, et al.* Drivers of Benthic Iron Fluxes and the Pore-Water Iron Isotopic Signature in Surface Sediments of South Georgia Fjords, Sub-Antarctica. *Global Biogeochemical Cycles* 40, e2025GB008856 (2026), https://doi.org/10.1029/2025GB008856.

50. Wunder LC, Aromokeye DA, Yin X*, et al.* Iron and sulfate reduction structure microbial communities in (sub-)Antarctic sediments. *ISME J* 15, 3587-3604 (2021), 10.1038/s41396-021-01014-9.

51. Lies DP, Hernandez ME, Kappler A*, et al.* Shewanella oneidensis MR-1 Uses Overlapping Pathways for Iron Reduction at a Distance and by Direct Contact under Conditions Relevant for Biofilms. *Appl Environ Microbiol* 71, 4414-4426 (2005), doi:10.1128/AEM.71.8.4414-4426.2005.

52. Gralnick JA, Bond DR. Electron Transfer Beyond the Outer Membrane: Putting Electrons to Rest. *Annu Rev Microbiol* 77, 517-539 (2023), https://doi.org/10.1146/annurev-micro-032221-023725.

53. Lovley DR. Dissimilatory Fe (III) and Mn (IV) reduction. *Microbiological reviews* 55, 259-287 (1991),

54. Oni OE, Miyatake T, Kasten S*, et al.* Distinct microbial populations are tightly linked to the profile of dissolved iron in the methanic sediments of the Helgoland mud area, North Sea. *Front Microbiol* 6, 365 (2015),

55. Riedinger N, Formolo MJ, Lyons TW*, et al.* An inorganic geochemical argument for coupled anaerobic oxidation of methane and iron reduction in marine sediments. *Geobiology* 12, 172-181 (2014), 10.1111/gbi.12077.

56. D'Hondt S, Inagaki F, Zarikian CA*, et al.* Presence of oxygen and aerobic communities from sea floor to basement in deep-sea sediments. *Nat Geosci* 8, 299–304 (2015), https://doi.org/10.1038/ngeo2387.

57. Mayer LM. Relationships between mineral surfaces and organic carbon concentrations in soils and sediments. *Chem Geol* 114, 347-363 (1994),

58. Zhao Y, Moore OW, Xiao K-Q*, et al.* The role and fate of organic carbon during aging of ferrihydrite. *Geochim Cosmochim Acta* 335, 339-355 (2022), https://doi.org/10.1016/j.gca.2022.07.003.

59. Zhao B, Yao P, Bianchi TS*, et al.* Preferential preservation of pre-aged terrestrial organic carbon by reactive iron in estuarine particles and coastal sediments of a large river-dominated estuary. *Geochim Cosmochim Acta* 345, 34-49 (2023), https://doi.org/10.1016/j.gca.2023.01.023.

60. Estes ER, Pockalny R, D'Hondt S*, et al.* Persistent organic matter in oxic subseafloor sediment. *Nat Geosci* 12, 126–131 (2019),

61. Cook AJ, Poncet S, Cooper APR*, et al.* Glacier retreat on South Georgia and implications for the spread of rats. *Antarct Sci* 22, 255-263 (2010), 10.1017/S0954102010000064.

62. Stimpfle J, Koch F, Ebner B*, et al.* Glacially derived iron is more bioavailable to Antarctic phytoplankton than other sources. *Communications Earth & Environment* 7, 89 (2026), 10.1038/s43247-025-03092-5.

63. Schwertmann U, Cornell RM. Ferrihydrite. In: *Iron Oxides in the Laboratory: Preparation and Characterization*). Second edn. WILEY‐VCH Verlag GmbH (2000).

64. Murphy KR, Stedmon CA, Graeber D*, et al.* Fluorescence spectroscopy and multi-way techniques. PARAFAC. *Anal Methods* 5, 6557-6566 (2013), https://doi.org/10.1039/C3AY41160E.

65. Ohno T. Fluorescence inner-filtering correction for determining the humification index of dissolved organic matter. *Environ Sci Technol* 36, 742-746 (2002),

66. Pucher M, Wünsch U, Weigelhofer G*, et al.* staRdom: Versatile Software for Analyzing Spectroscopic Data of Dissolved Organic Matter in R. *Water* 11, 2366 (2019), 10.3390/w11112366.

67. Gesing TM, Robben L. Determination of the average crystallite size and the crystallite size distribution: the envelope function approach EnvACS. *Journal of Applied Crystallography* 57, 1466-1476 (2024), https://doi.org/10.1107/s1600576724007362.

68. Howell RC, Proffen T, Conradson SD. Pair distribution function and structure factor of spherical particles. *Physical Review B* 73, 094107 (2006), 10.1103/PhysRevB.73.094107.

69. Stookey LL. Ferrozine---a new spectrophotometric reagent for iron. *Anal Chem* 42, 779-781 (1970),

70. Cline JD. Spectrophotometric determination of hydrogen sulfide in natural waters 1. *Limnol Oceanogr* 14, 454-458 (1969),

71. Zhu Q-Z, Yin X, Taubner H*, et al.* Secondary production and priming reshape the organic matter composition in marine sediments. *Science advances* 10, eadm8096 (2024), 10.1126/sciadv.adm8096.

Supplementary Information for

Natural organic matter coating on iron oxide changes its role in carbon preservation in marine sediments

Yunru Chen[1,2]*, Heidi Taubner[1,3], Verena Heuer[1,3], Jenny Altun[1,3], Rianne van Kaam[1], Lars Robben[4,5,6], Wolfgang Bach[1,3], Lea C. Wunder[2], Graciana Willis-Poratti[7,8], Anna Helms[2], Sabine Kasten[1,3,9], Matthias Zabel[1], Kai-Uwe Hinrichs[1,3], Michael W. Friedrich[1,2]

1. MARUM-Center for Marine Environmental Sciences, University of Bremen, Bremen, Germany

2. Microbial Ecophysiology Group, Faculty of Biology/Chemistry, University of Bremen, Bremen, Germany

3. Faculty of Geosciences, University of Bremen, Bremen, Germany

4. Solid State Chemical Crystallography, Faculty of Biology/Chemistry, Bremen, Germany

5. Data Science Center, University of Bremen, Germany

6. MAPEX – Center for Materials and Processes, University of Bremen, Germany

7. Instituto Antártico Argentino, Buenos Aires, Argentina

8. Consejo Nacional de Investigaciones Científicas y Técnicas, Buenos Aires, Argentina

9. Alfred Wegener Institute Helmholtz Centre for Polar and Marine Research, Bremerhaven, Germany

*Corresponding author: yunruchen@marum.de

This file includes:

Supplementary Table 1

Supplementary Figure 1-8

Supplementary Data 1-2

Supplementary Table 1. Constrained fates of ^{13}C-acetate in the incubations. Data are presented as means ± standard deviation (n = 3).

Uncoated Fh incubation						
	Acetate (no Fh protection)		Acetate+Fh[a] (partial Fh protection)		Acetate+Fh+molybdate (full Fh protection)	
	Concentration (μM)	Percentage (%)	Concentration (μM)	Percentage (%)	Concentration (μM)	Percentage (%)
Remineralized	66 ± 3	57 ± 3	40 ± 2	35 ± 2	30 ± 3	26 ± 3
In supernatant[b]	BDL	BDL	BDL	BDL	11 ± 1	9 ± 1
Associated with solid phases	50 ± 3	43 ± 3	76 ± 2	65 ± 2	76 ± 3	65 ± 3
Total	116	100	116	100	116	100
NOM-coated Fh incubation						
	Acetate (no Fh protection)		Acetate+Fh[a] (partial Fh protection)		Acetate+Fh+molybdate (full Fh protection)	

	Concentration (μM)	Percentage (%)	Concentration (μM)	Percentage (%)	Concentration (μM)	Percentage (%)
Reremineralized	66 ± 3	56 ± 2	54 ± 3	46 ± 2	6 ± 0	5 ± 0
In supernatant[b]	0 ± 1	0 ± 1	BDL	BDL	7 ± 1	6 ± 1
Associated with solid phases	51 ± 2	44 ± 2	64 ± 3	54 ± 2	104 ± 1	89 ± 1
Total	118	100	118	100	118	100

[a] For all the treatments testing partial Fh protection, we selected the one with only abiotic iron reduction, which means Fh was added within a dialysis bag.

[b] The concentration of total acetate in some treatments were below the detection limit (BDL = 9 μM), and therefore, the calculated concentrations of added acetate in the supernatant were taken as zero in these cases for further calculations.

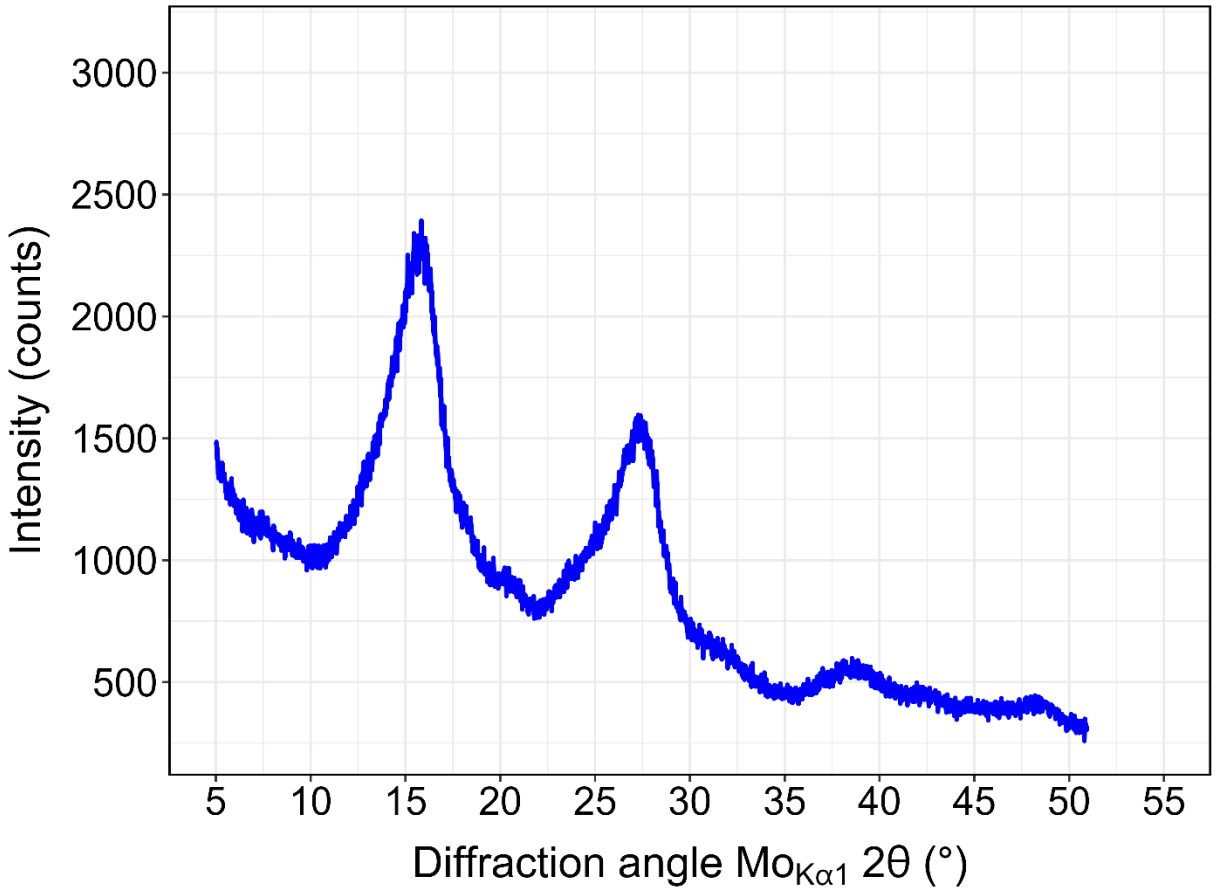

Supplementary Figure 1. The X-ray diffraction (XRD) pattern, recorded using Mo Kα1 radiation, of the synthesized 2-line ferrihydrite used in this study. Peak positions are given as 2θ.

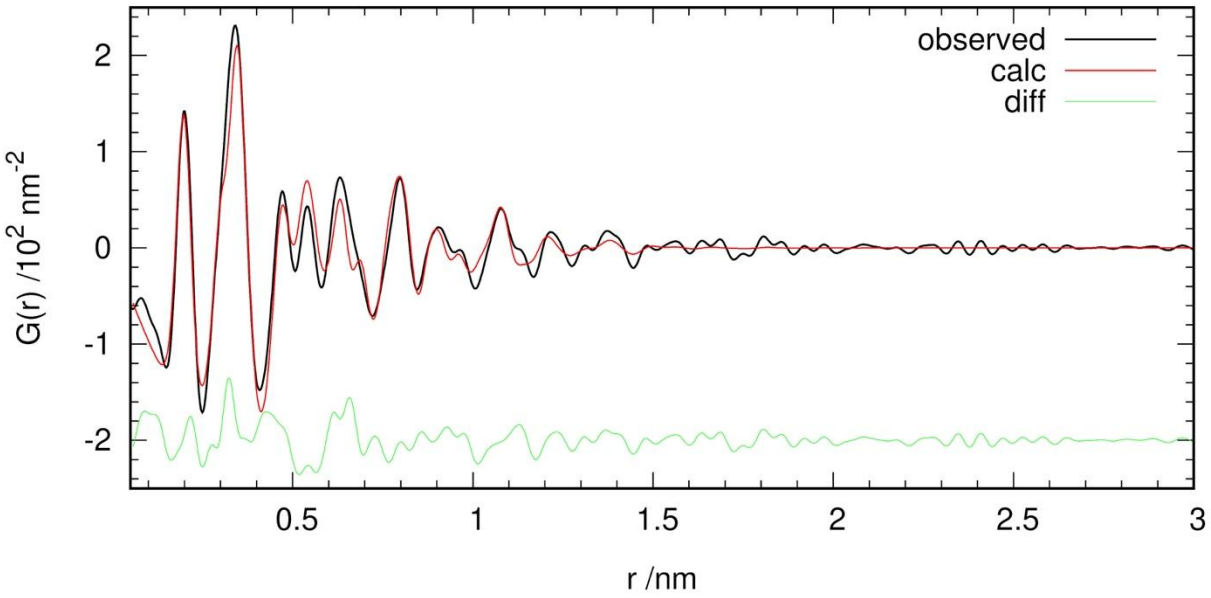

Supplementary Figure 2. The G(r) of the Fh (black), along with a refinement using the structure model of Michel et al. (red) and their difference (green). The structure model fits the data quite well, confirming the structure of two-line Fh.

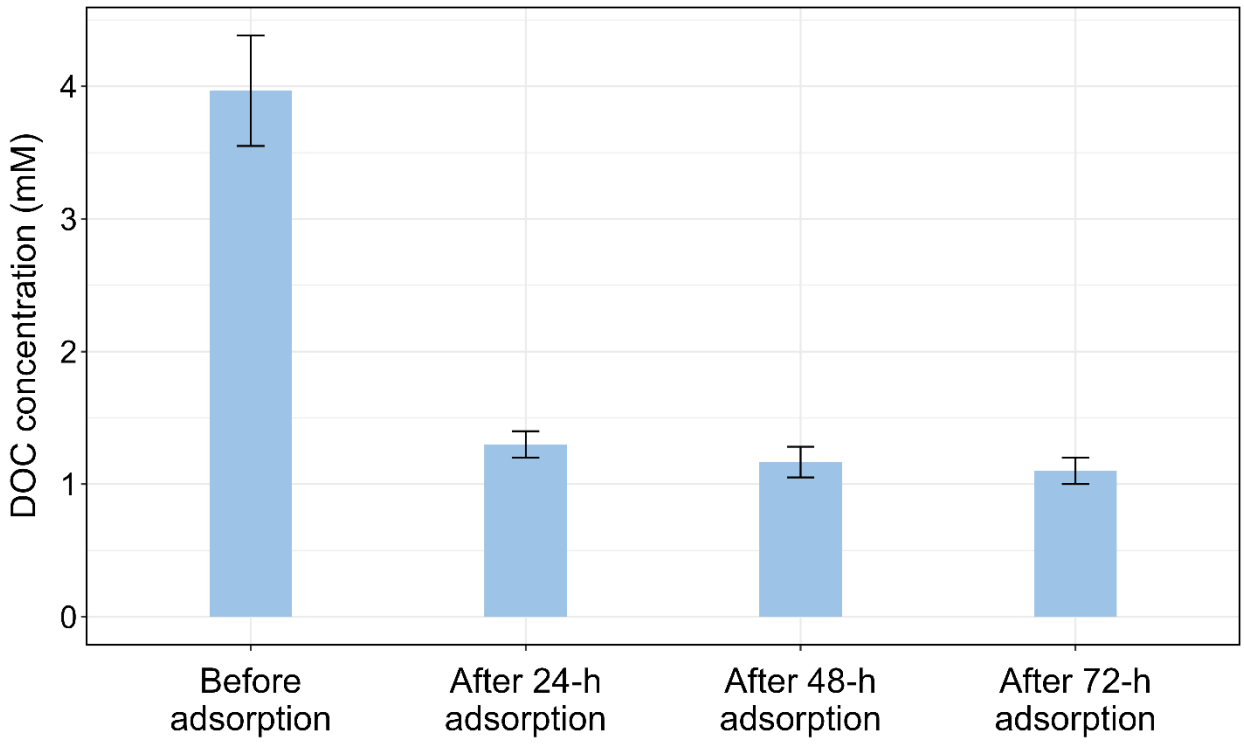

Supplementary Figure 3. Dissolved organic carbon (DOC) concentration in the supernatant during a 72-h adsorption experiment using nature organic matter (NOM) solution extracted from marine sediments and ferrihydrite (Fh). Each treatment was

performed in triplicates. Bars represent mean DOC concentrations, and error bar indicate the standard deviation of the triplicates.

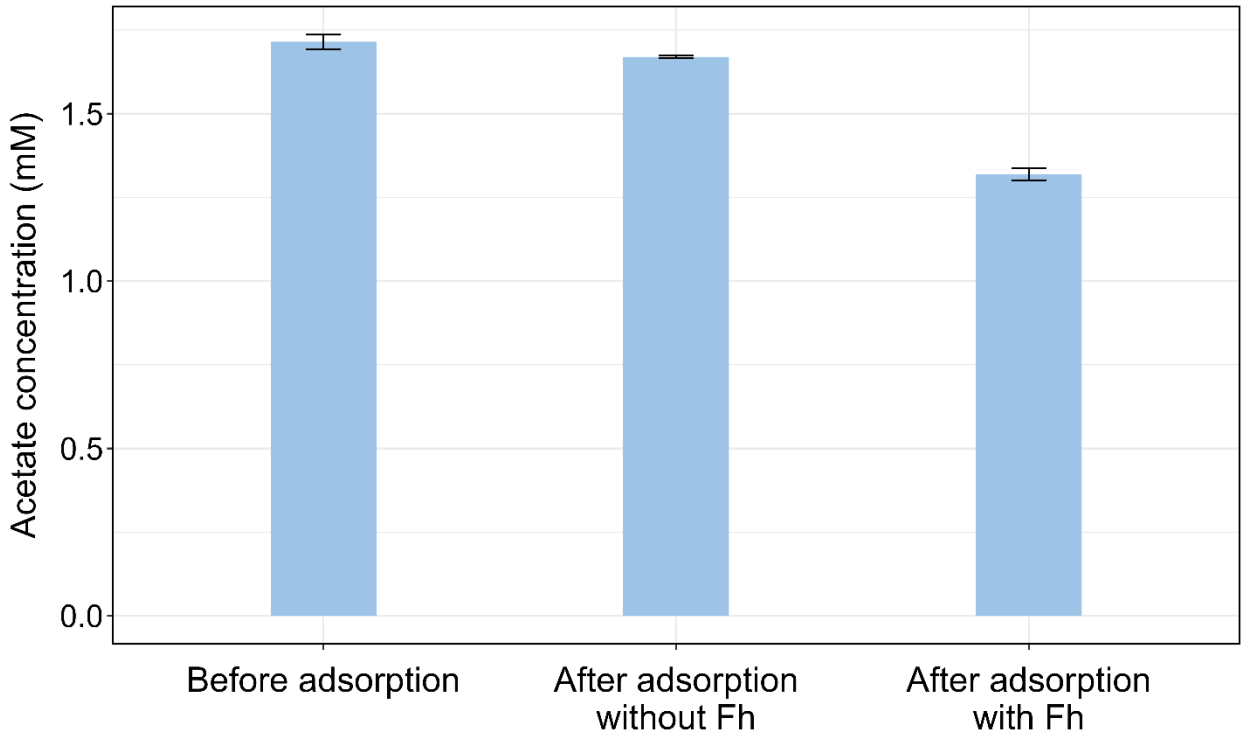

Supplementary Figure 4. Acetate concentration before adsorption and in the supernatant after adsorption after 24 hours using acetate solution and ferrihydrite (Fh). Each treatment was performed in triplicates. Bars represent mean DOC concentrations, and error bar indicate the standard deviation of the triplicates (n = 3). The acetate adsorbed on Fh was determined as the difference in acetate concentration between treatments with and without Fh after 24 h of adsorption, as adsorption of acetate on the tubes was observed in the tube with only acetate solution.

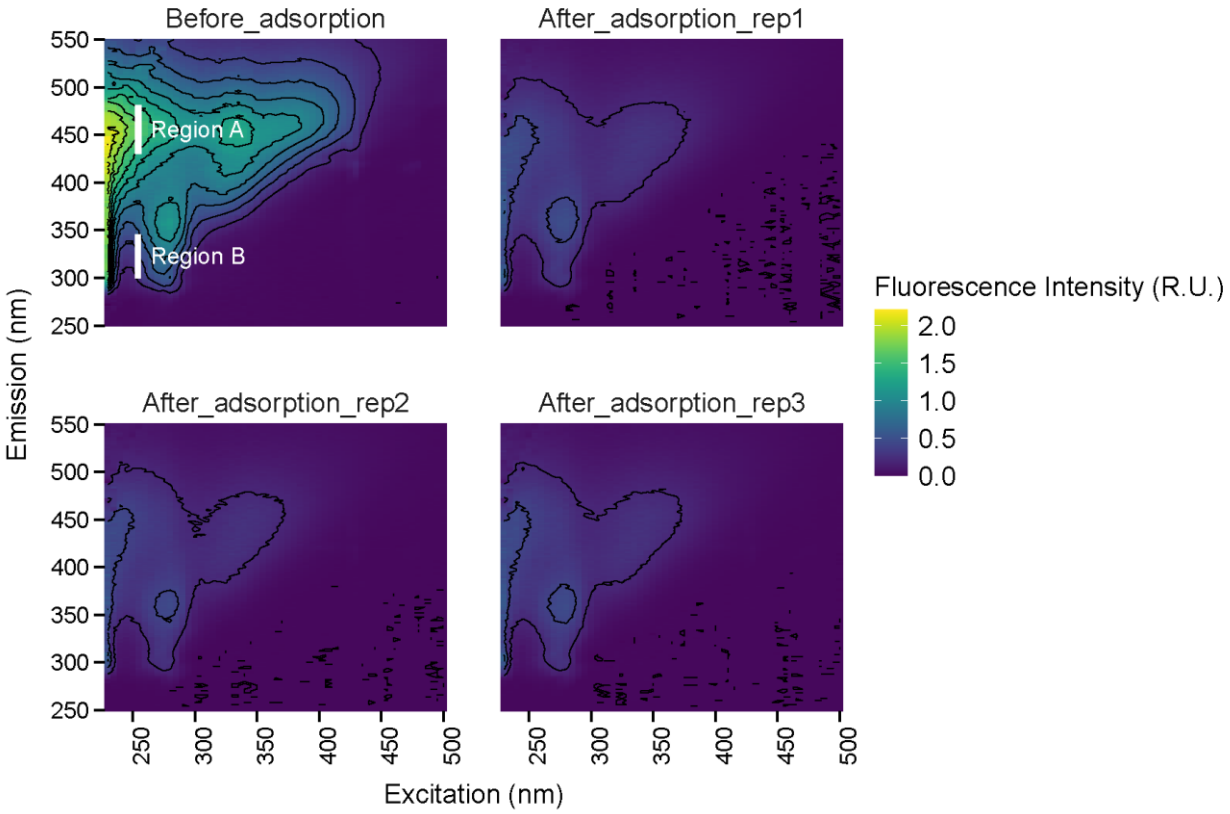

Supplementary Figure 5. Three-dimensional excitation emission matrices (EEMs) of the NOM solution before adsorption and of the supernatant after the adsorption experiment with ferrihydrite. “rep1”, “rep2” and “rep3” represent three replicates. The HIX is defined as the fluorescence intensity in the 435 - 480 nm region (Region A) divided by the sum of intensity in the 300 - 345 nm (Region B) and 435 - 480 nm regions at the excitation wavelength of 254 nm. The fluorescence intensity decreased dramatically after the adsorption experiment, indicating a substantial adsorption of humic-like NOM on Fh.

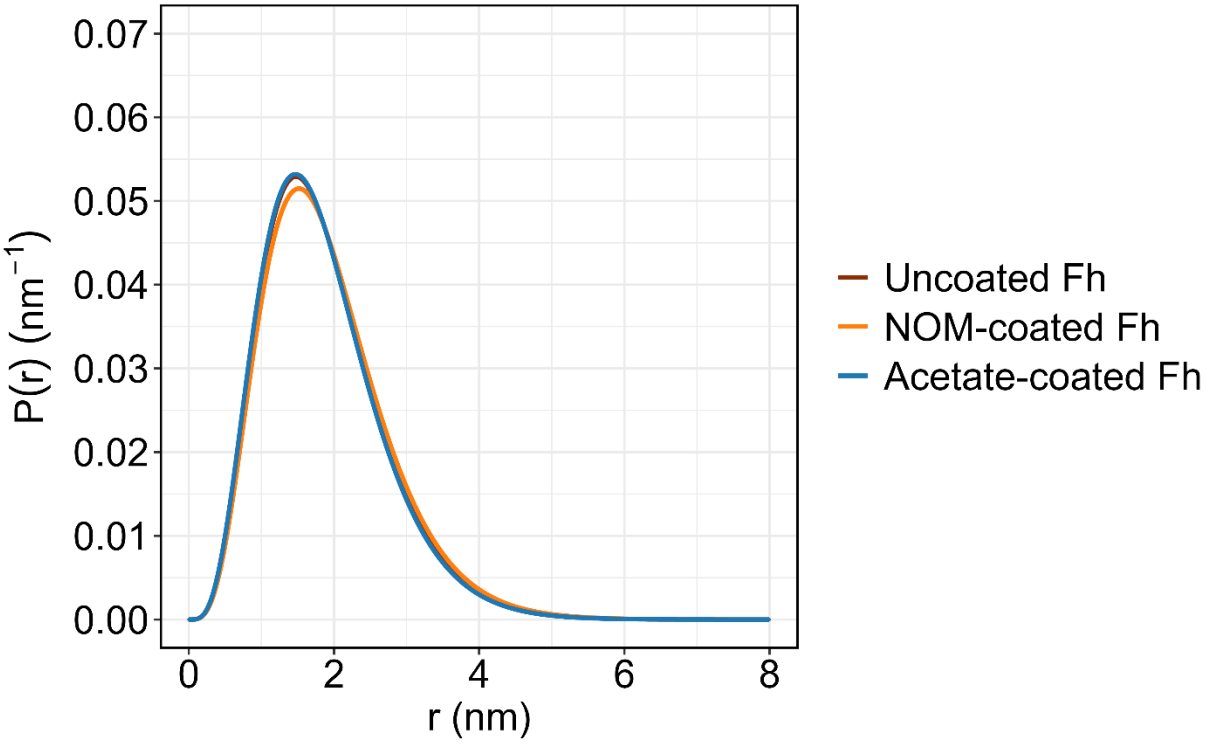

Supplementary Figure 6. Distribution functions of the average crystallite size *P(r)* of uncoated Fh (black), NOM-coated Fh (red), and acetate-coated Fh (blue). The x-axis shows the crystallite radius *r* in nanometers, and the y-axis shows the distribution density *P(r)*.

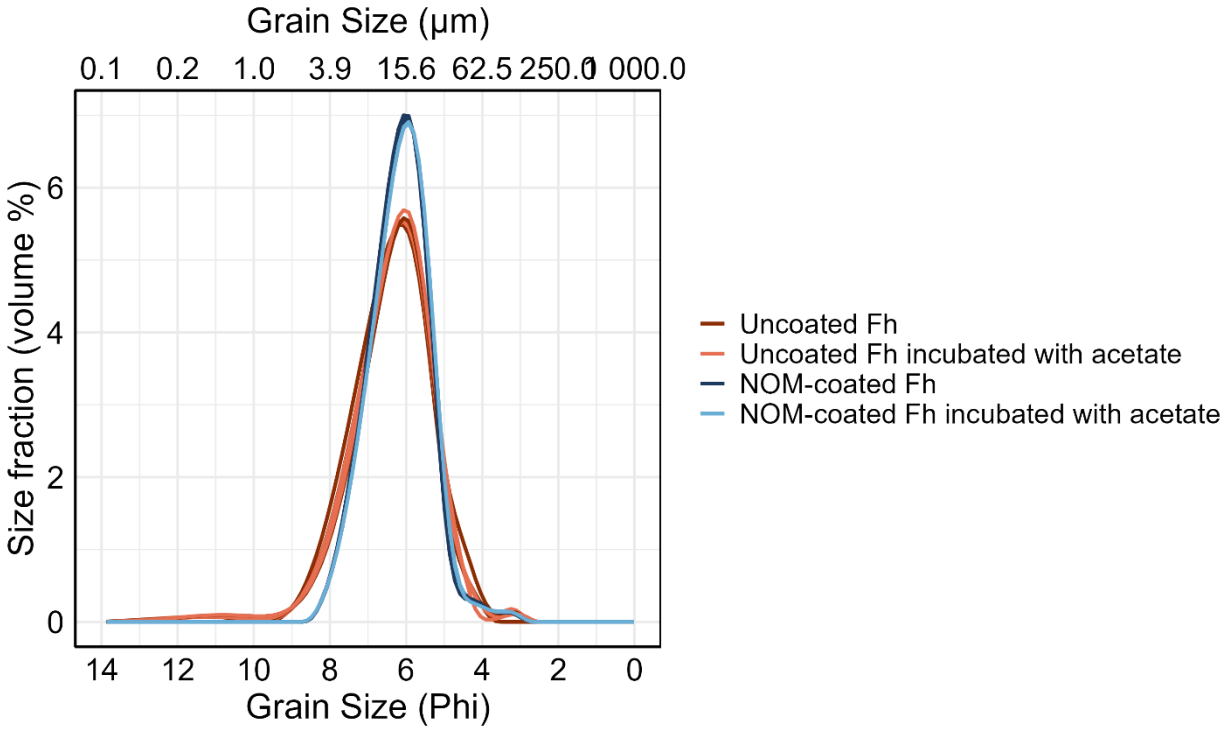

Supplementary Figure 7. The particle size distribution of uncoated Fh, NOM-coated Fh, uncoated Fh incubated with acetate, and NOM-coated Fh incubated with acetate. Three replicates were prepared and measurement for each treatment.

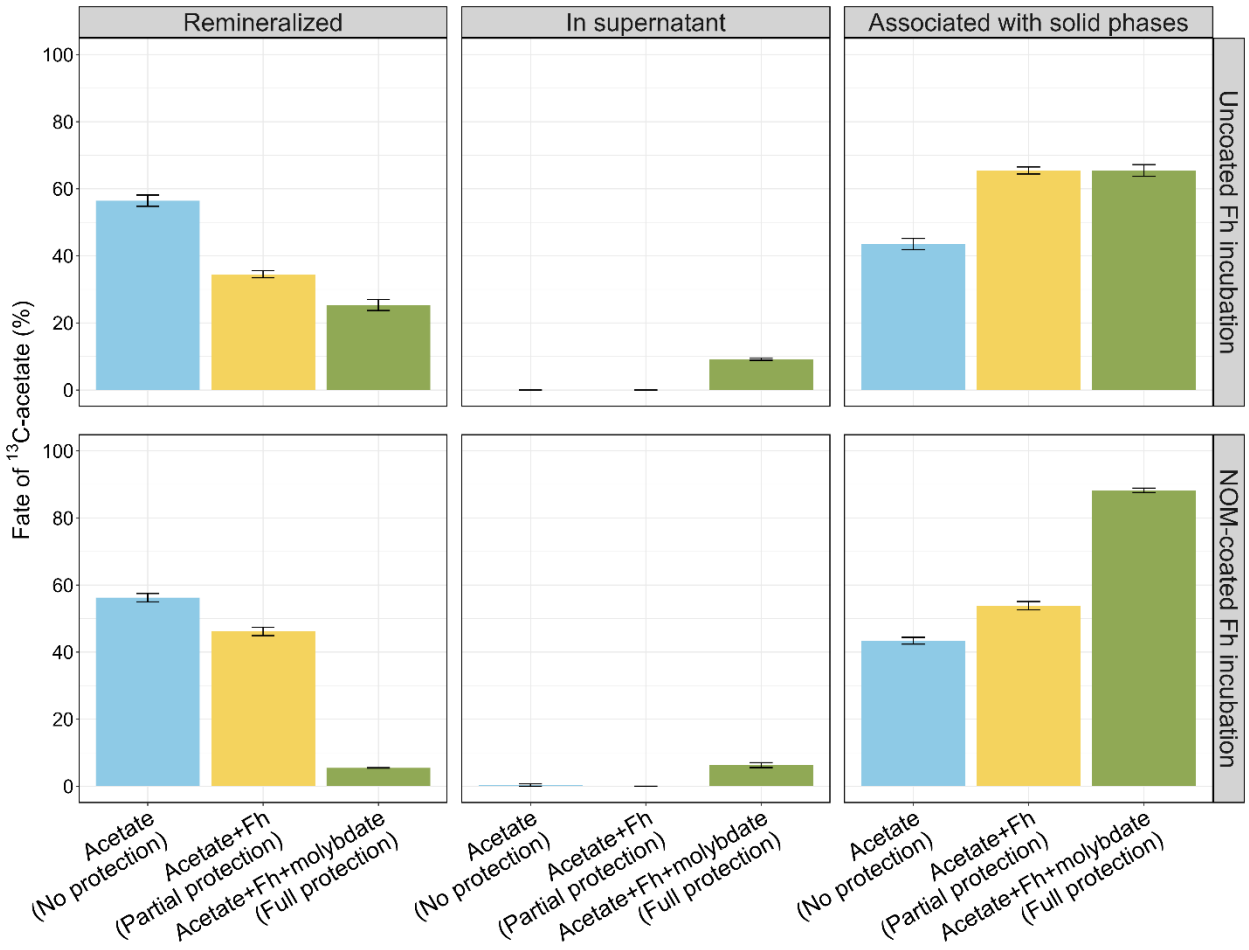

Supplementary Figure 8. Fates of ^{13}C-acetate in uncoated and NOM-coated Fh incubations. In all the treatments shown here, Fh was first added into a dialysis bag before adding into the sediments to exclude most biotic iron reduction. Therefore, "Partial protection" means Fh protection with abiotic iron reduction to remobilize Fh-associated ^{13}C-acetate. Bars show mean percentages of ^{13}C-acetate remineralized, remained in the supernatant, and protected by solid phases, with error bars indicating the standard deviation of incubation replicates (n = 3).